Master Thesis in Physical Oceanography

Topographically Controlled Flow in the Isfjorden Trough and the West Spitsbergen Shelf

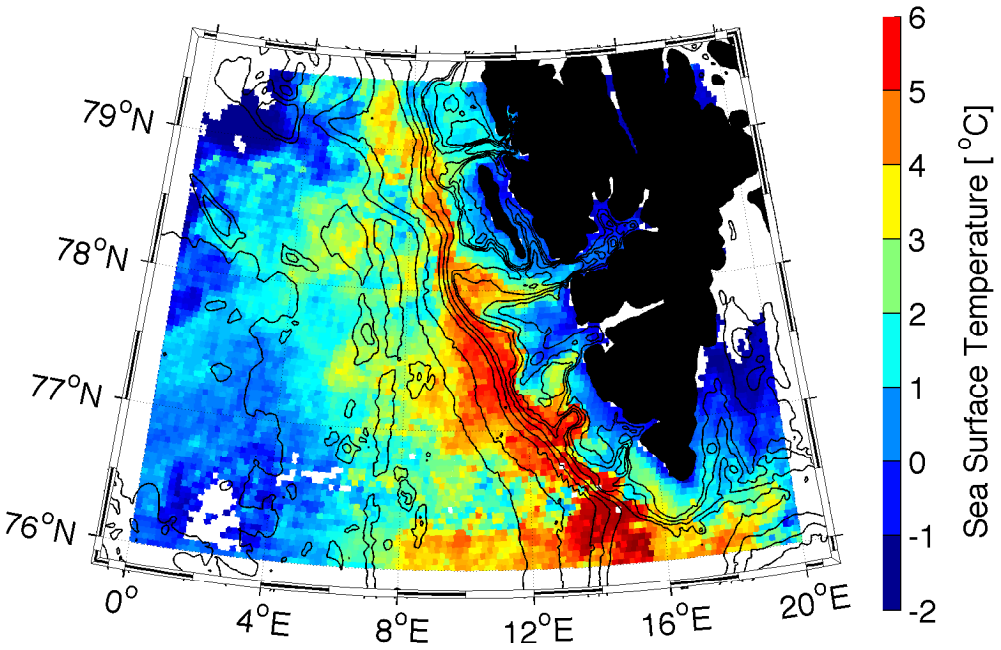

Juni Vaardal-Lunde

November 2011

UNIVERSITY OF BERGEN
GEOPHYSICAL INSTITUTE

UNIS

Acknowledgments

First of all I would like to thank my one and only, supervisor Frank Nilsen. Thanks for letting me write my master thesis here in beautiful Svalbard and for letting me take part of real and exciting science. Thanks for always being up for a chat, keeping my motivation up and letting me participate in your world of equations and numerical thinking, it is actually quite interesting. Also thanks for letting me come along on two cruises. This was a great experience where I learned a lot and even got to call myself a teacher.

I would also like to thank Sigurd H. Teigen for helping me with questions I did not manage to formulate and for reading through and improving my thesis. I really appreciated your great help. Also a great thanks to Berit Jakobsen, the librarian at UNIS, that found all I could ever need of literature and was always up for a chat when I was stuck at something. Thanks to Eva Sessford for willingly reading through my thesis.

The 3 o'clock coffee group (Tiina, Stephan and Thomas), you were a great motivation for staying at UNIS passed 4, almost every day.

I would also like to thank my partner Max, for all his patience during the last year, for listening to all the weird stuff I manage to think about and for always being there for me. Also thanks for reading my thesis at least a thousand times.

Thanks to my four parents and one brother for their loving support during my semesters in Bergen and Svalbard.

And last but not least, the super nice dogs of Frank and Ragnheid. Bamse, Vargtass, Micky and Bris listened to all my thoughts without complaining and gave me many funny moments to remember.

Juni Vaardal-Lunde
Longyearbyen, 16 November 2011

Abstract

A one layer numerical model demonstrates how the Atlantic Water (AW) from the West Spitsbergen Current (WSC) is topographically steered onto the West Spitsbergen Shelf (WSS) with a special emphasise on the Isfjorden Trough. Model results show that the WSC connects easier to the Isfjorden Trough than anywhere else on the shelf, letting the trough be exposed to warm and salty AW. When increasing the maximum velocity of the WSC more inflow into the troughs and consequently onto the WSS is observed in the model. The flow tends to follow steeper bathymetry when we increase the maximum velocity of the WSC and the topographical guiding is Rossby number dependent. Where isobaths converge, so will the streamlines, indicating stronger flow over steeper topography. This will increase the velocity shear and force the flow to follow deeper isobaths while circulating the troughs. The model is used to explain the January 2006 event, where an accumulation of warm water could be found in Isfjorden due to southerly winds. The simple one layer barotropic model gives a good approximation of the dynamical processes on the WSS, which plays a significant role in the cooling process of the WSC on its way to the Arctic Ocean.

Contents

Chapter 1

Introduction

The Northern branch of the Norwegian Atlantic Current, which is the northward extension of the Gulf Stream, splits up south of Bear Island [Blindheim and Østerhus, 2005] into the Barents Sea Branch (BSB) and the slope confined West Spitsbergen Current (WSC). The WSC forms the major pathway of warm and salty Atlantic Water (AW) to the Arctic Ocean. The current flow through the Fram Strait [Schauer et al., 2004], located between the Svalbard archipelago and Greenland. The WSC flowing along the west coast of Svalbard and into the Arctic Ocean keeps the east Fram Strait ice free, also during winter. On the western side of the Fram Strait, the East Greenland Current (EGC) transports fresher and colder water out of the Arctic Ocean. The EGC is also the main exporter of sea ice from the Arctic. The Fram Strait is the area where the majority of oceanic mass, heat and salt exchange between the Arctic Ocean and the rest of the world's oceans occur as it is the only deep water passage between the Arctic Ocean and the sub-polar oceans [Boyd and D'Asaro, 1994]. The Fram Strait is a key feature when looking at the large scale world ocean circulation. The Arctic Ocean is linked to the global climate [Gascard et al., 1995] and since the Arctic is more climatically sensitive than other areas, changes in the climate system are more apparent and its connection to the surrounding oceans is therefore an interesting study area.

The WSC is steered by the topography in the Fram Strait and splits up into at least three branches. One branch known as the Return Atlantic Current (RAC) re-circulates to the Greenland Sea near or in the Fram Strait, while the two other branches bifurcate further north at around 79.5°N. One branch follows the western slope of the Yermak plateau before continuing north of Svalbard and is referred to as the Yermak branch. The Yermak branch is largely re-circulated and rapidly loses its AW signal due to mixing with ambient waters around the Yermak Plateau [Gascard et al., 1995]. The other branch flows north close to the shelf break of Spitsbergen before it turns eastward and crosses the Yermak Plateau. This third branch is referred to as the Svalbard branch [Schauer et al., 2004; Manley, 1995]. The remainder of the Yermak branch and the Svalbard branch rejoin somewhere north east of Svalbard. When reaching the St. Anna Trough between Franz Josef's Land and Novaja Zemlja, they flow together with the

colder Barents Sea branch along the Arctic Basin rim and ridges [Teigen, 2011]. The Svalbard branch is considered to be the major conveyor of AW to the Arctic Ocean [Saloranta and Haugan, 2001], and Schauer et al. [2004] found a very strong increase in heat transport to the north connected with the WSC, while no compensating signal was found in the southward flow. The net heat transport to the north implies that heat remains in the Arctic Ocean, which could lead to warming of the Arctic directly coupled to the Arctic Ocean heat budget. The importance of the heat transport in the WSC and the cause of the recent warming of the subsurface Arctic Ocean and reduction of sea ice is further discussed by Schauer et al. [2004]; Zhang et al. [1998]; Cokelet et al. [2008] and Polyakov et al. [2010].

Due to its impact on the oceanic net heat transport to the Arctic Ocean, it is of vital importance to understand the key processes that lead to transformation of the WSC through exchange with the shelf and fjord waters west of Svalbard [Cottier et al., 2005]. Boyd and D'Asaro [1994] discuss plausible mechanisms for cooling the WSC, and attempt to quantify the contributions from atmospheric cooling, ice melt and isopycnal mixing. The results indicate that the WSC loses more heat than could be explained by direct heat loss to the atmosphere and melting ice. Saloranta and Haugan [2004] and Nilsen et al. [2006] estimate the heat loss in the subsurface layer between 100 and 500 meters of the upper slope domain west of Spitsbergen to be 2.5-3 times as large as the heat loss estimated for the upper 100 meters surface layer. Exchange between the colder shelf water and the WSC at the slope is pointed to as the primary mechanism for the cooling in the subsurface layer. Saloranta and Svendsen [2001] suggest that topographical steering (i.e. the current follows depth contours), due to conservation of potential vorticity, is guiding the AW from the slope and onto the shelf through cross shelf troughs. In recent years more studies on the cross shelf exchange on the West Spitsbergen Shelf (WSS) have been published [Saloranta and Haugan, 2001, 2004; Cottier et al., 2007; Nilsen et al., 2008], with a focus on the shelf exchange between Arctic Water (ArW) and AW from the WSC [Nilsen et al., 2006; Teigen et al., 2010]. Cross-front and shelf exchange may occur due to isopycnal eddy diffusion by topographic vorticity waves [Nilsen et al., 2006; Teigen et al., 2010], causing warm water from the WSC to enter the shelf area while colder shelf water is mixed into the core of WSC, resulting in a net heat loss of the WSC.

The year 2005/2006 was related to high air temperatures and little sea ice extent. Extensive flooding of the coastal waters with AW from the WSC increased the shelf water temperature and caused unusually little sea ice extent in the fjords on the west coast of Spitsbergen. Cottier et al. [2007] demonstrate that the shelf response to the dynamical effect of wind forcing has a profound effect on the heat content of the shelf water. Along-shelf winds can cause flooding of AW on the shelf area, inhibiting the sea ice formation, thus causing local warming in Spitsbergen.

The focus of this thesis is to study topographical effects on the WSC and the shelf dynamics. A one layer model is developed to examine the processes related to inflow of AW onto the

WSS, with a special emphasise on the Isfjorden Trough, by looking mainly at different maximum velocities of the WSC. Also the cross-shelf location of the current maximum in the WSC may affect the amount of inflowing water. The model results are compared with the situation discussed by Cottier et al. [2007]. The inflow of warm and salty water is exposed to colder air temperatures on the WSS, leading to cooling of the water by a heat loss to the atmosphere as well as the surrounding water.

The general ocean circulation west of Spitsbergen and the WSC is described in Chapter 2, together with hydrographical data from the Isfjorden Trough area. Further, theory and method are presented in Chapter 3 with focus on the different model parameters. The conservation of heat along the path of the inflowing AW is also addressed. The numerical model is elaborated in Chapter 4. Model results are presented in Chapter 5 and finally the model results and the heat estimates are discussed in Chapter 6.

Chapter 2

Site and observations

2.1 General circulation

The Svalbard archipelago is situated between 76-81°N and 10-34°E with Spitsbergen being its largest individual island. The main circulation pattern of the currents flowing west of Spitsbergen is shown in Figure 2.1. The WSC leading AW to the Arctic Ocean can be seen as the red line from the south (Figure 2.1), following the continental shelf break west of Spitsbergen. The RAC is represented by recirculating. leaving the WSC to the west. On the shelf, colder and relatively fresh ArW transported in the upper layer flows northward with the coastal current and is represented as the blue line (Figure 2.1). The current flows from Storfjorden, around the southern tip of Spitsbergen before crossing the Isfjorden Trough [Svendsen et al., 2002]. The separation between AW from the WSC at the continental shelf break and ArW from the Coastal Current on the West Spitsbergen Shelf (WSS) is referred to as the Arctic Front [Saloranta and Svendsen, 2001]. The Arctic front is a subsurface temperature and salinity front (TS-front) observed near the upper slope of the shelf break west of Spitsbergen (Figure 2.1, black dashed line). Cross shelf exchange of AW and ArW have been revealed by CTD measurements from 1998 to 2000 by Saloranta and Svendsen [2001], and estimated heat loss implies that the dynamics of the WSC plays a significant role in the cooling of the WSC before entering the Arctic Ocean [Nilsen et al., 2006].

2.2 The West Spitsbergen Current (WSC)

The WSC (Figure 2.1, red line) is highly barotropic with a smaller baroclinic shear and has a relatively steady north-northwest flow [Fahrbach et al., 2001; Teigen et al., 2010]. The approximate depth of the warm core in the WSC is located between 200-250 m depth, with a faster and broader flow during winter and a more moderate flow during summer [Teigen et al., 2010]. The average velocity of the WSC during winter (determined as the vertical average of the velocity profile) is found to be 0.20 ms^{-1} [Fahrbach et al., 2001; Saloranta and Haugan, 2004; Teigen et al., 2010], but the current velocity can occasionally exceed 0.50 ms^{-1} during the

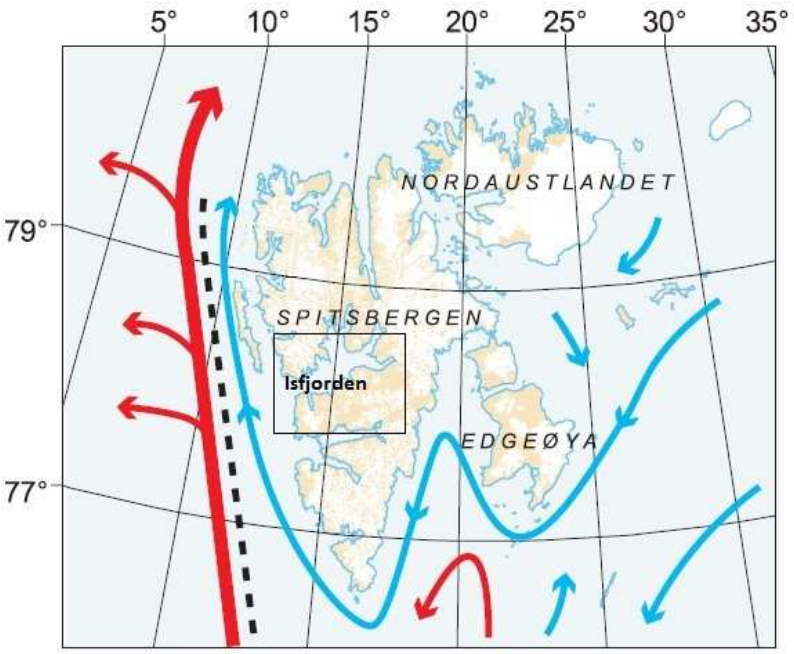

Figure 2.1: The major currents around Svalbard [Svendsen et al., 2002]. The WSC is shown by the red line and the coastal current is represented by the blue line. The black dashed line separating the currents is called the Arctic front.

winter months, with the fastest flow observed from early January to mid-April [Teigen et al., 2010]. A current meter mooring section is situated across the eastern Fram Strait covering the upper WSS west of the Kongsfjorden Trough. The mooring section has been maintained by the Alfred Wegener Institute since 1997 as part of the European Union project VEINS (1997-2000), ASOF-N (2002-2005) and EU-DAMOCLES (2006-) [Fahrbach et al., 2001; Schauer et al., 2004, 2008]. An additional mooring F0 was installed in September 2007 by the International Polar Year project Integrated Arctic Ocean Observing System (iAOOS) Norway [Teigen et al., 2010]. The time variation of the northward current speed in the WSC is shown in Figure 2.2, where Figure 2.2a is the horizontal current profile from September 2005 to August 2006 from mooring F1 to F7 at a depth range between 230 m to 260 m (mooring F3 did not work during the entire period and is therefore marked as red). Figure 2.2b is a time evolution of the fitted background current profile from November 2007 to June 2008 from mooring F0 to F4 calculated by Teigen et al. [2010]. The background current represents the WSC at the 200 to 250 m layer where the maximum velocity is found between mooring F1 and F2. The fastest flow, which also has the widest shape, is found both years from January to late April in 2006 and to middle March in 2008. In February 2006 and 2008 the WSC narrows and weakens before it again increases and widens in March. During the summer period, the WSC is weaker.

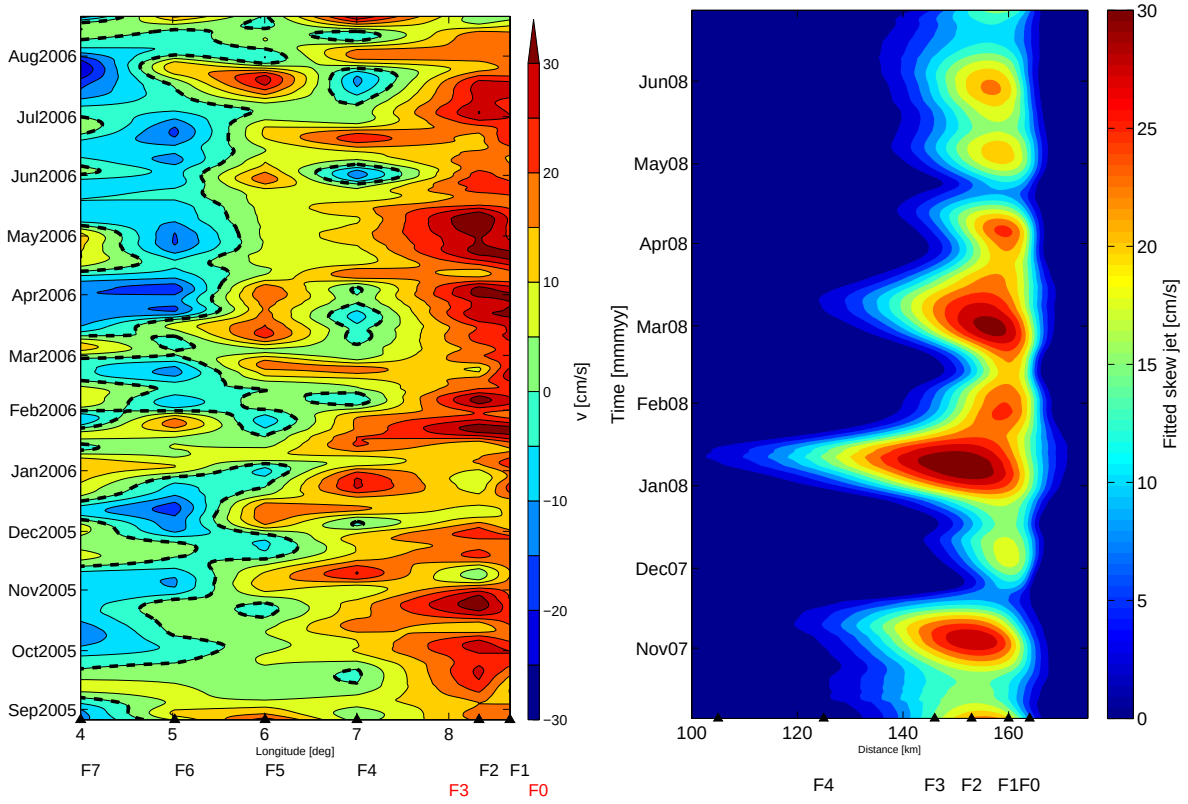

(a) (b)

Figure 2.2: Hovemöller diagram of a) the WSC from September 2005 to August 2006 at a depth between 230-260 m and b) the fitted skew jet profile, from November 2007 to June 2008, at the 200-250 m level at F0-F4, from Teigen et al. [2010]. Mooring positions are marked in both the figures. Mooring F0 was not installed in 2005 and 2006 and mooring F3 only measured in the beginning of the measuring period (both marked as red in Figure 2.2a).

2.3 Isfjorden and the Isfjorden Trough

Isfjorden, located on the western side of Spitsbergen and with an angle of 60° in a north east direction, is by area the largest fjord in the archipelago [Nilsen et al., 2008]. Isfjorden splits up into two fjords, Nordfjorden to the north and Sassenfjorden to the east, both of which split up into two minor fjords. Ekmanfjorden and Dicksonfjorden make up the northern arms of Nordfjorden, and Sassenfjorden divides into Billefjorden and Tempelfjorden (Figure 2.3). Freshwater input to the fjord is mainly from calving and ablation of glaciers, sea ice melt, river run off and precipitation, during the summer months. Most of the glaciers can be found on the northern side of the fjord, and it is assumed that the most important freshwater sources are from calving and ablation of glaciers [Nilsen et al., 2008].

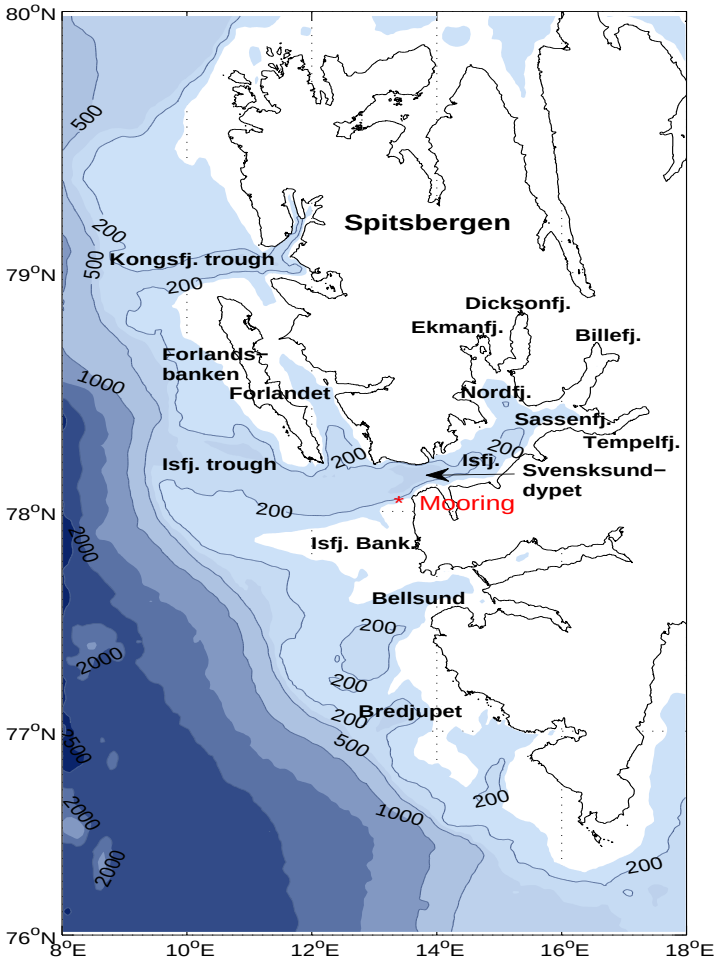

Figure 2.3: Map of Spitsbergen. Arrow represents the location of Svensksunddypet and Forlandet is short for Prins Karls Forland. Depth contours in [m].

Sea ice conditions in Isfjorden are highly seasonal with freezing periods from late November to mid-May, and no ice during summer. Fast ice can be found in the inner part of the fjords, while the rest is mainly frazil ice and some drift ice entering from the shelf areas [Nilsen et al., 2008].

Isfjorden has no sill, hence there is no topographical restriction against direct contact with the continental shelf water through the Isfjorden Trough. The trough is located as a depression cutting across the WSS from the shelf break to the fjord, and has a significant affection on the mean circulation, being able to steer the AW topographically from the WSC and into the trough. The Isfjorden Trough is the deepest on the west coast of Spitsbergen and reaches down

to 200-300 meter. The fjord systems' deepest point can be found in the mouth of Isfjorden, Svensksunddypet at 455 meters, while the depth of the Isfjorden Bank is less than 100 meters.

2.3.1 Hydrography of the Isfjorden Trough

Data for analysing the water masses around the Isfjorden Trough were collected using a SeaBird Electronics SBE 911-plus CTD, measuring conductivity, temperature and depth. Hydrographic cross sections from the shelf area and Isfjorden, covering the WSS and the trough region, where measured during a cruise with R/V Mosby September 2010 and R/V Lance April 2011. The different water masses found around Svalbard and west of Spitsbergen are classified by temperature and salinity, described in Table 2.1 after the definitions by Swift and Aagaard [1981] and Saloranta [2001]. Along the continental shelf of Spitsbergen AW is found as part of the WSC, which is warm ($> 3°C$) and saline (> 34.9) compared to other water masses found in the Arctic. Through contact with the atmosphere and surrounding water masses the AW cools down and when the temperature drops below 3°C, Lower Arctic Intermediate Water (LAIW) is formed. The LAIW is mostly found beneath the AW. Polar Water (PW), representing the surface water during summer, can be transported south from the Polar Regions or locally formed by melting of sea ice and glaciers. The PW is generally fresh (< 34.4) and is in this region only found during summer. Due to the large seasonal temperature variation on the West Spitsbergen Shelf, it is necessary to elaborate upon the formation of the water masses in the salinity range between 34.4 and 34.9, in this thesis defined as Spitsbergen Shelf Water (SSW). SSW is found during summer and winter, but is derived from different water masses depending on the season. During summer warm and salty AW from the WSC mixes with the colder and fresher PW creating the summer SSW that is generally found beneath the PW and mainly located at the shelf. Warming from the atmosphere and the sun also affect the SSW found during summer. During winter, atmospheric cooling of the SSW found in summer, AW and the LAIW can be sources to the SSW found during winter. The SSW is also influenced by the coastal current transporting colder and fresher water from east of Svalbard, modified from the East Spitsbergen Current.

Table 2.1: Water masses described by Swift and Aagaard [1981] and Saloranta [2001].

Water masses	**Initials**	**Temperature range [°C]**	**Salinity range**
Atlantic Water	AW	> 3	> 34.9
Lower Arctic Intermediate Water	LAIW	< 3	> 34.9
Polar Water	PW		< 34.4
Spitsbergen Shelf Water	SSW		$34.4 < S < 34.9$

A TS diagram shown in Figure 2.4, represents water masses from CTD section 2 south of Prins Karls Forland (see section 2 in Figure 2.5), indicating that the hydrographic conditions on the shelf and trough area are highly seasonal. The red dots represent the summer values, from September 2010, and the black dots represent the winter values, from April 2011. During sum-

mer (Figure 2.4, red dots) AW and SSW dominate the section, some PW can also be found. During winter (Figure 2.4, black dots) SSW classify most of the water masses, while small amounts of LAIW can be found. The observations are spread along the mixing line between SSW at the freezing point and AW, although no observations of actual AW and freezing SSW were made at this section.

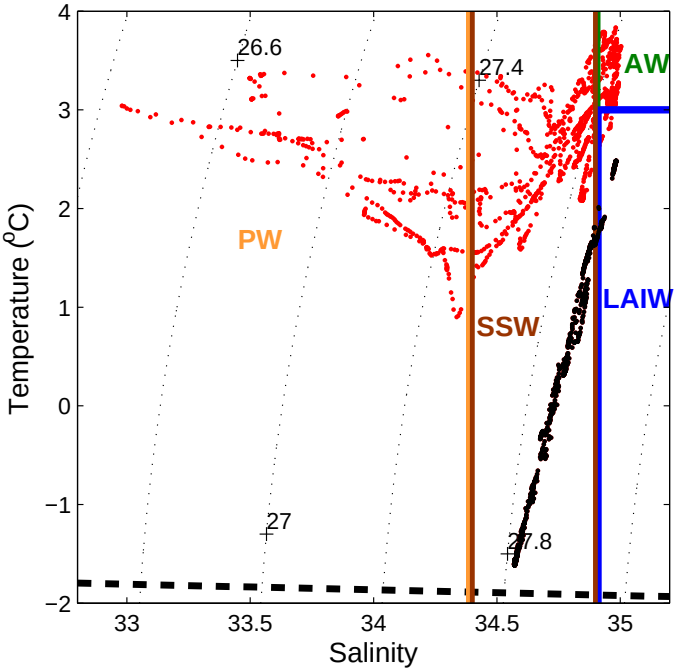

Figure 2.4: Temperature and Salinity diagram (TS-diagram), showing the different water masses during summer 2010 (red dots) and winter 2011 (black dots) from CTD section 2 marked in Figure 2.5. The different water masses are separated with colour boxes and the abbreviations are explained in Table 2.1. Dotted lines represent isolines of potential density (σ_θ [kg m^{-3}]) and the dashed line denotes the freezing point.

The CTD sections shown in Figure 2.5 from September 2010, are mainly taken over the Isfjorden Trough, making it possible to trace the AW entering the trough area. The same sections are taken during April 2011, but note that the two southernmost stations in section 1 and 3 had to be cancelled due to heavy ice conditions. CTD data from September 2010, referred to as the summer profiles, are shown in Figure 2.6 and CTD data from April 2011, referred to as the winter profiles, are shown in Figure 2.7. The three red lines (Figure 2.6) represent ADCP sections at three different depths, and are further discussed in section 2.3.2. The summer profiles show AW in all sections. At section 1, in the outer part of the trough, the AW is found below 50 m from station 232 to 229 (Figure 2.6a and 2.6b) and below 100 m from station 229 and 228. At section 2 (Figure 2.6c and 2.6d) the AW is concentrated bellow 75 m from stations 192 to 44. It is interesting to see how the water on the shelf area at stations 195 and 196 is colder and fresher than at station 44, which is taken over the southern slope of the Isfjorden Trough. At station

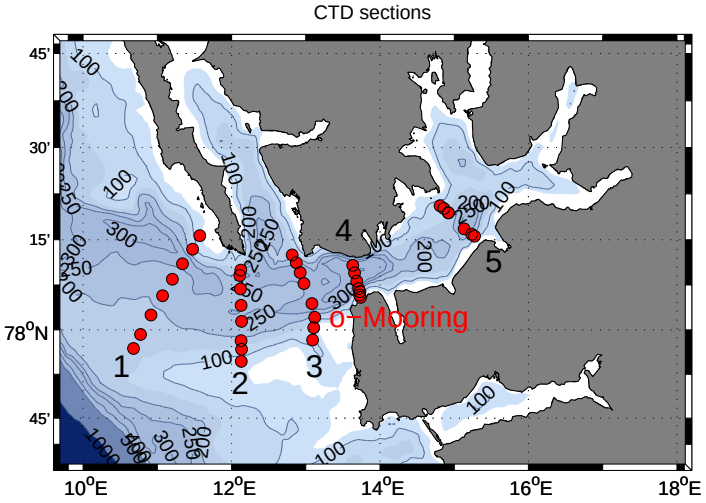

Figure 2.5: Map over CTD stations in the Isfjorden Trough and fjord system from the cruise with R/V Mosby September 2010. Mooring I, discussed in Section 2.3.2, is marked. Only data from section 1,2 and 3 will be studied.

194, salinity up to 35 with a temperature of 3.5°C can be found. This is defined as proper AW entering the trough at around 140 m. A return flow out of the trough seem to be controlled by a combination of a surface elevation pressure gradient and the thermal wind relation as seen by the density plot in Figure 2.8, where relatively warm and salty water can be seen below 150 m depth in section 2 at station 192 (Figure 2.6c and 2.6d). At section 3 (Figure 2.6e and 2.6f), close to Isfjorden, the AW can be located below 150 m, mainly at station 203. In the northern part of all the summer profiles from September 2010, a colder and fresher core of water flowing westward and out of the trough can be found at 50 to 100 m depth.

The winter profiles (Figure 2.7) show warmer and more saline AW entering the Isfjorden Trough on the southern side, while on the northern side colder and less saline water is leaving the trough area. Section 1 (Figure 2.7a and 2.7b) has a homogeneous warm and salty water column on the southern side, with a less homogeneous, cold and fresher water column on the northern side. At stations 229 and 230, salinities of 35 can be found with a temperature of 2.5°C. From section 2 (Figure 2.7c and 2.7d), as in September 2010, the warmest and most saline water is found at station 44 with colder and fresher water at stations 195 and 196. The water column is still homogeneous in the southern part of the trough, with a less homogeneous water column in the northern part. From section 3 (Figure 2.7e and 2.7f) the warmest and most saline water is found below 100 m with the highest temperature and salinity at station 202. The homogeneous water columns found in section 1 and 2 are not found in section 3. In the entrance and in the middle part of the trough (section 1 and 2) during winter, the water column is highly homogeneous on

the southern side with the same temperature, salinity and density in the whole water column and containing mostly LAIW. The northern part of section 1 and 2 and the inner part of the trough, section 3, show more stratification resulting in a less homogeneous water column with changing temperature and salinity with depth.

The stratification parameter, $S^{\frac{1}{2}}$, representing the baroclinic shear in the water column and being the ratio of the depth scale to the e-folding scale, λ^{-1}, is defined as

$$S^{\frac{1}{2}} = \frac{ND}{fL}$$

and

$$\lambda^{-1} = \frac{fL}{N} = \frac{D}{S^{1/5}}.$$

The Brunt-Väisälä frequency $N = -\sqrt{\frac{g}{\rho}\frac{\partial \rho}{\partial z}}$ is estimated from the CTD data (density plots from section 2 shown in Figure 2.8), D is the depth scale indicated by the depth at the shelf break, f is the Coriolis parameter and L is the length scale given by the distance AW is able to penetrate the Isfjorden Trough from the position of the maximum current in the WSC. When $S^{\frac{1}{2}}$ is close to one, the water column is controlled by the stratification. If $S^{\frac{1}{2}} << 1$ and $\lambda^{-1} >> D$, the water column is close to barotropic with only a small baroclinic shear. In order to define the stability of the water sections from September 2010 and April 2011 the Brunt-Väisälä frequency is calculated from the CTD data at section 2 (stations 191, 193 and 44), to give an overview of the stratification across the Isfjorden Trough. From the Brunt-Väisälä frequency the stratification parameter and the e-folding scale are calculated, shown in Table 2.2.

Table 2.2: The Brunt-Väisälä frequency found from a selections of CTD stations by taking the mean over the entire water column. Stratification parameter, $S^{\frac{1}{2}}$, and vertical e-folding scale, λ^{-1}, are calculated from the Brunt-Väisälä frequency N when D = 500 m, L = 80 km and the Coriolis parameter for 78°N.

	Summer			**Winter**		
Station number	Sta191	Sta193	Sta44	Sta191	Sta193	Sta44
Mean N^2	$6.2{\cdot}10^{-5}$	$5.0{\cdot}10^{-5}$	$5.8{\cdot}10^{-5}$	$2.4{\cdot}10^{-6}$	$1.2{\cdot}10^{-6}$	$1.2{\cdot}10^{-6}$
Mean N [s^{-1}]	$7.8{\cdot}10^{-3}$	$7.0{\cdot}10^{-3}$	$7.6{\cdot}10^{-3}$	$1.5{\cdot}10^{-3}$	$1.1{\cdot}10^{-3}$	$3.5{\cdot}10^{-4}$
$S^{\frac{1}{2}}$	0.342	0.307	0.007	0.002	0.001	<0.001
λ^{-1} [m]	1500	1600	1500	7700	10 400	32 400

From the stratification parameter it can be found that the winter section is much more barotropic than the summer section, in agreement with the CTD measurements (Figure 2.6 and 2.7). The stratification parameter indicates that the Isfjorden Trough is highly barotropic during winter, with the most barotropic conditions in the southern part of the trough, linked to the inflow of water.

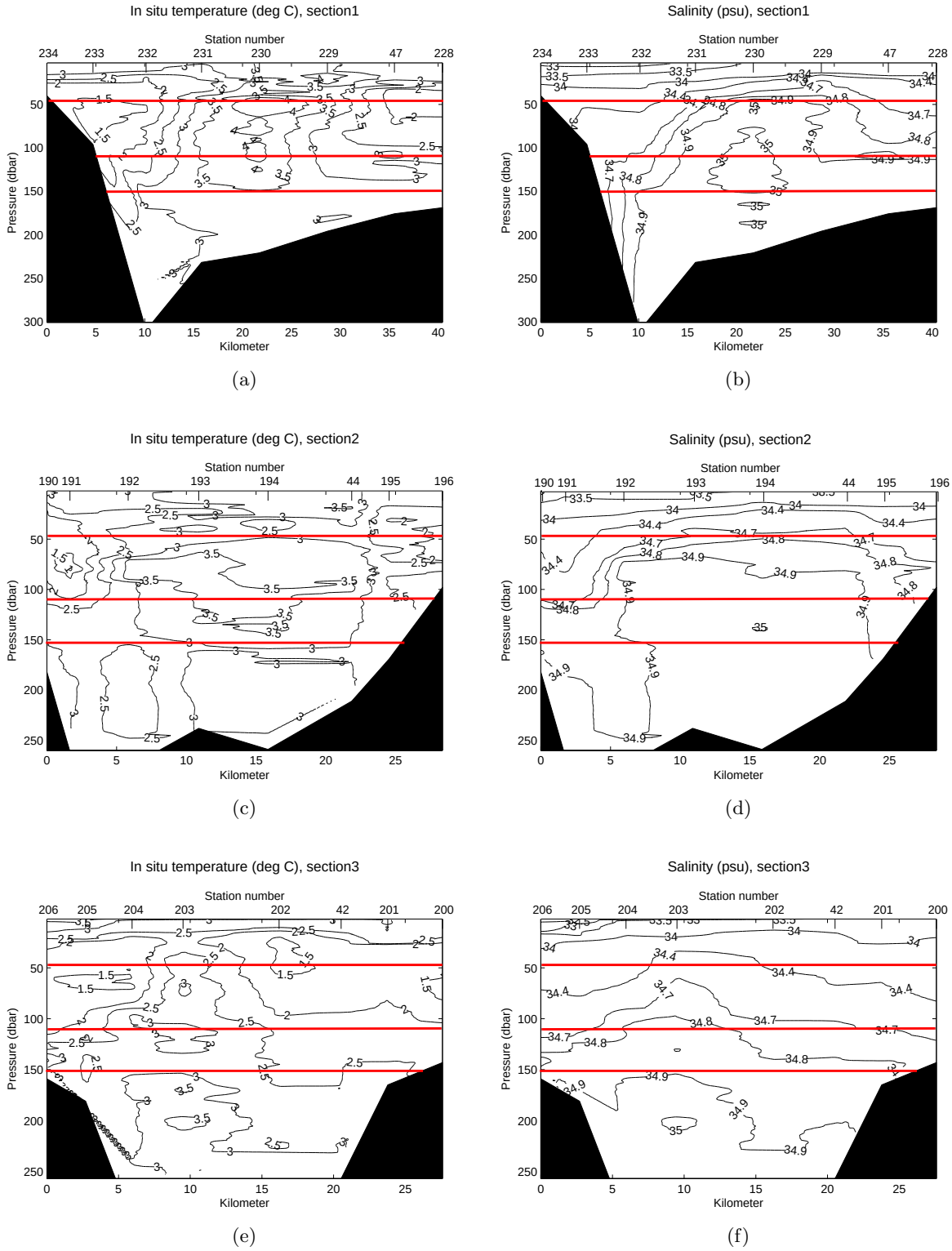

Figure 2.6: CTD sections from September 2010. North is to the left side and south is to the right side. a) Temperature section 1, b) Salinity section 1, c) Temperature section 2, d) Salinity section 2, e) Temperature section 3, f) Salinity section 3. Red lines indicate the depth of the ADCP measurements discussed in section 2.3.2.

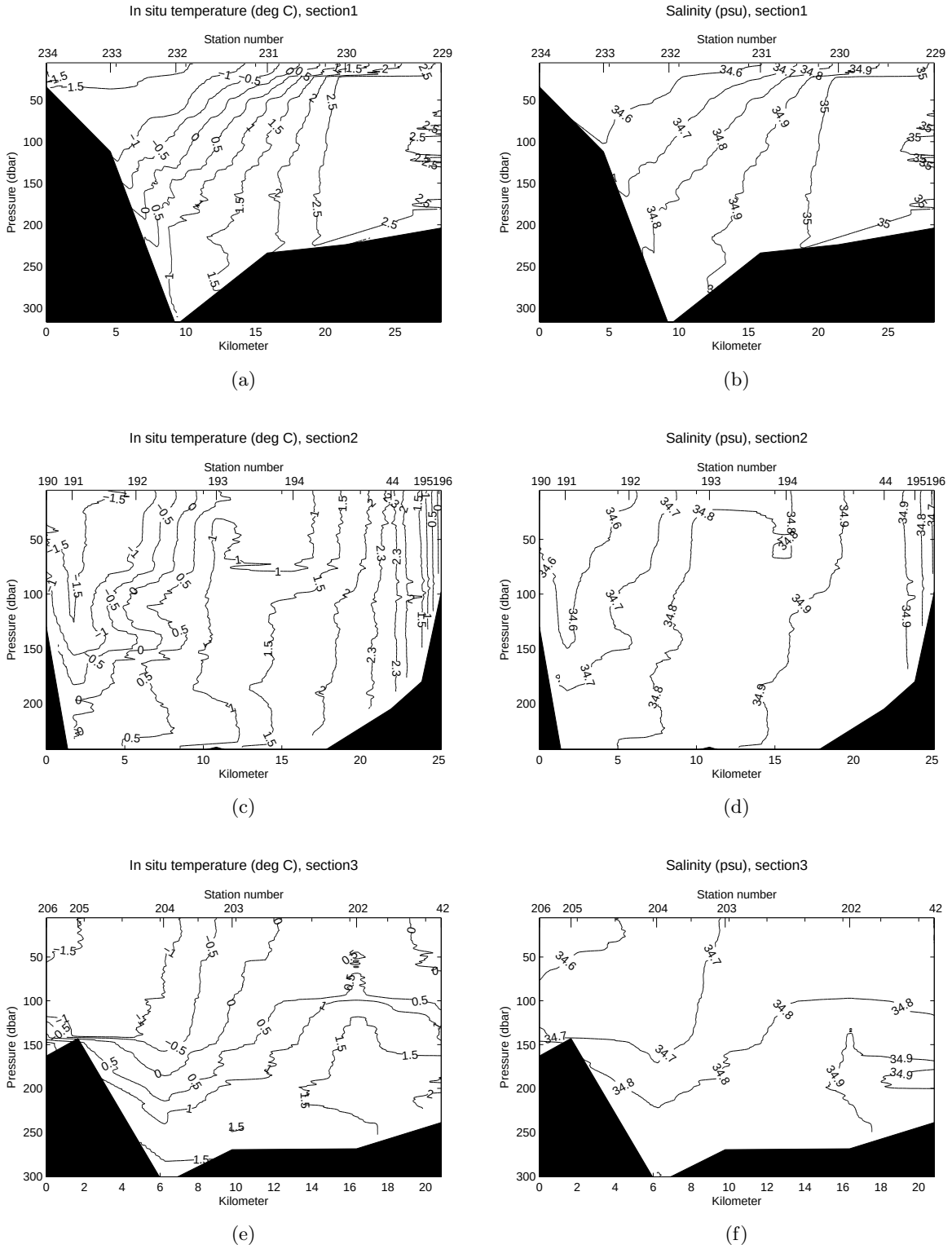

Figure 2.7: CTD sections from April 2011. North is to the left side and south is to the right side. a) Temperature section 1, b) Salinity section 1, c) Temperature section 2, d) Salinity section 2, e) Temperature section 3, f) Salinity section 3.

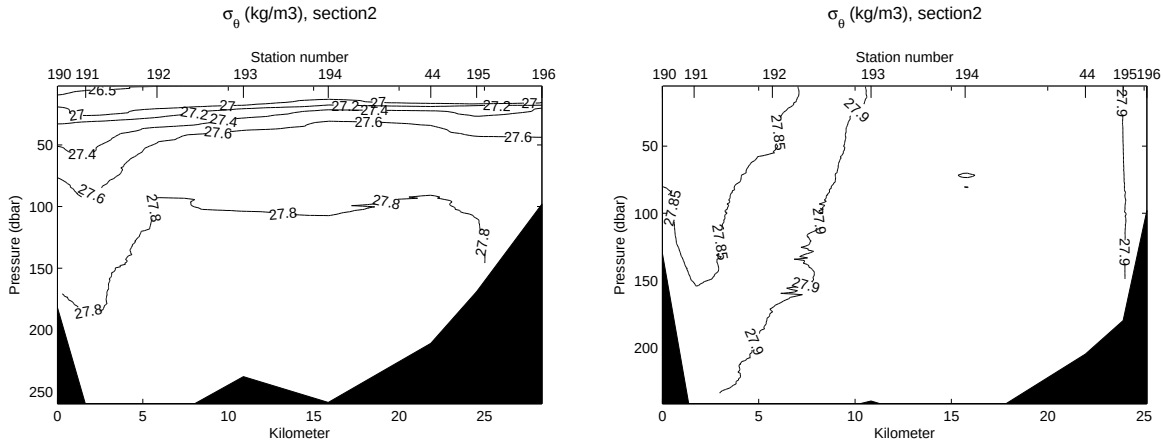

(a) (b)

Figure 2.8: CTD sections showing the density. North is to the left side and south is to the right side. a) Density for section 2, September 2010, b) Density for section 2, April 2011.

2.3.2 Current measurements

A cyclonic circulation pattern can be found in the Isfjorden Trough from Acoustic Doppler Current Profiler (ADCP) data from R/V Mosby (September 2010), with inflow and outflow of water in the Isfjorden Trough (Figure 2.9). The black dots represent the CTD section 1, 2 and 3 from September 2010. Figure 2.9a shows the current at a depth bin between 44.4 to 48.4 m, Figure 2.9b shows the current from 108.4 to 112.4 m and Figure 2.9c represents the current between 148.4 m to 152.4 m. The mid part of the trough, south of Prins Karls Forland, has an inflow on the southern side and an outflow on the northern side in all the three levels. The inner ADCP section shows a more northerly flow, linked to the coastal current on the shelf. Figure 2.9 also demonstrates how the current mainly follows the isobaths in the outer part of the trough, with a higher velocity on the northern side. West of Prins Karls Forland the flow has a northern direction, showing how the outflow from the Isfjorden Trough continues northward towards the Arctic Ocean. The three red lines in the CTD data from Figure 2.6 represent the ADCP section at 46 m, 110 m and 150 m being the average depth of the ADCP measurements. A dominating barotropic situation is, as for the CTD sections, found on the southern side of the Isfjorden Trough.

Current data in the Isfjorden Trough is also found by a Mooring I stationed in the entrance of Isfjorden at 200 m depth at position 78.037°N and 13.314°E, collecting data from September 2005 to September 2006 (for Mooring I location, see Figure 2.5). Mooring I data is discussed by Cottier et al. [2007] and a description of the mooring can be found in Table 2.3. Figure 2.10 shows the in- and out-fjord current over one year for 50 and 182 m depth, where positive values correspond to in-fjord current direction and negative values describe out-fjord current direction. The in- and out-fjord directions are calculated to be an angle of 60° to north-east direction,

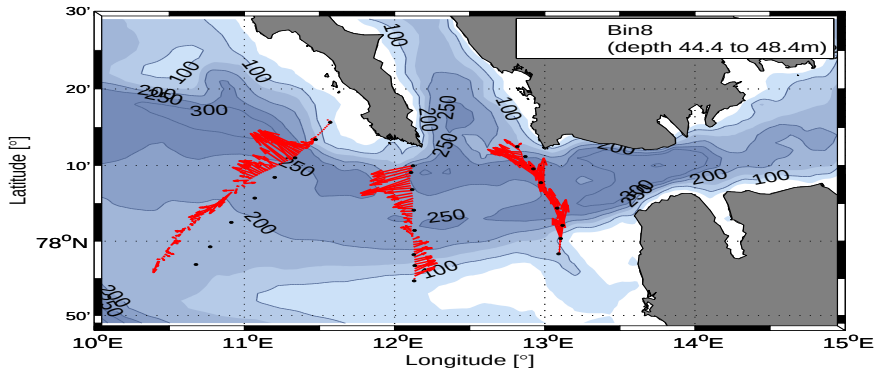

(a)

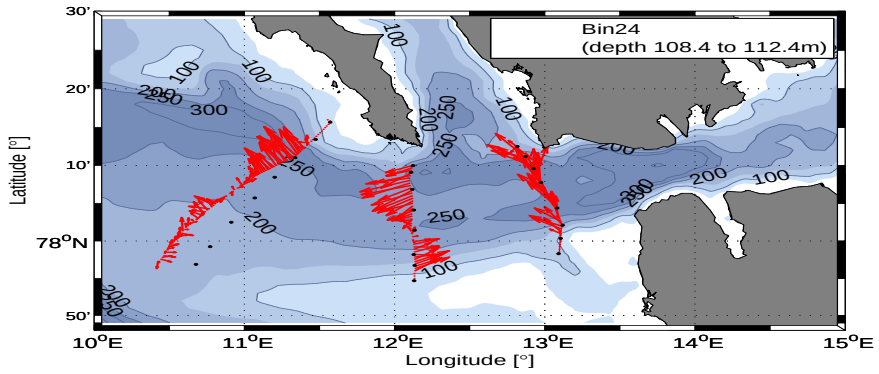

(b)

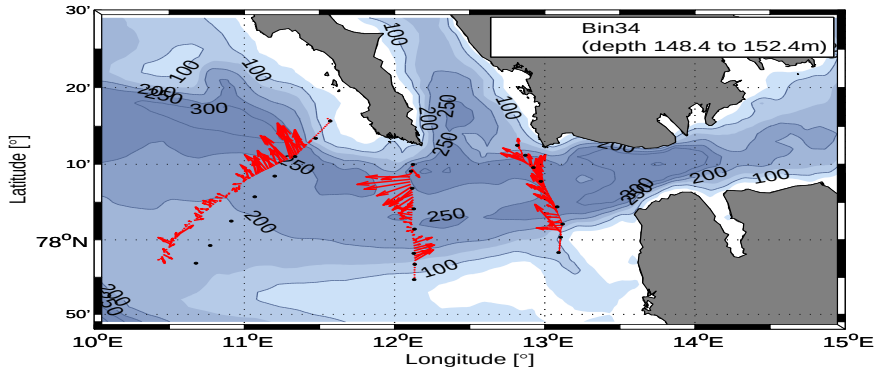

(c)

Figure 2.9: ADCP current data for flow in the layer between a) 44.4 and 48.4 m, b) 108.4 and 112.4 m and c) 148.4 and 152.4 m. Black dots show the CTD section from September 2010. The maximum current velocity observed in the figure is approximately 0.50 ms^{-1}.

Table 2.3: Details of Mooring I at position 78.037°N and 13.314°E at 200 m depth. The measurements are done from September 2005 to September 2006.

	Depth [m]	**Parameters**
RCM777	50	u,v,T,p,Tur
RCM780	182	u,v,T,S,p,Tur
WRL7	195	T,p

Parameters: u, east velocity; v, north velocity; T, temperature; S,salinity; p,pressure; Tur, turbidity.

corresponding with the direction of the trough and fjord in the Isfjorden entrance where the mooring is located. The border between inflow and outflow is marked with a black dashed line. The main current is found to be directed in-fjord with a maximum velocity around 0.50 ms^{-1} during February. The in-fjord current has a higher velocity during winter then summer, found from both 50 and 182 m depths.

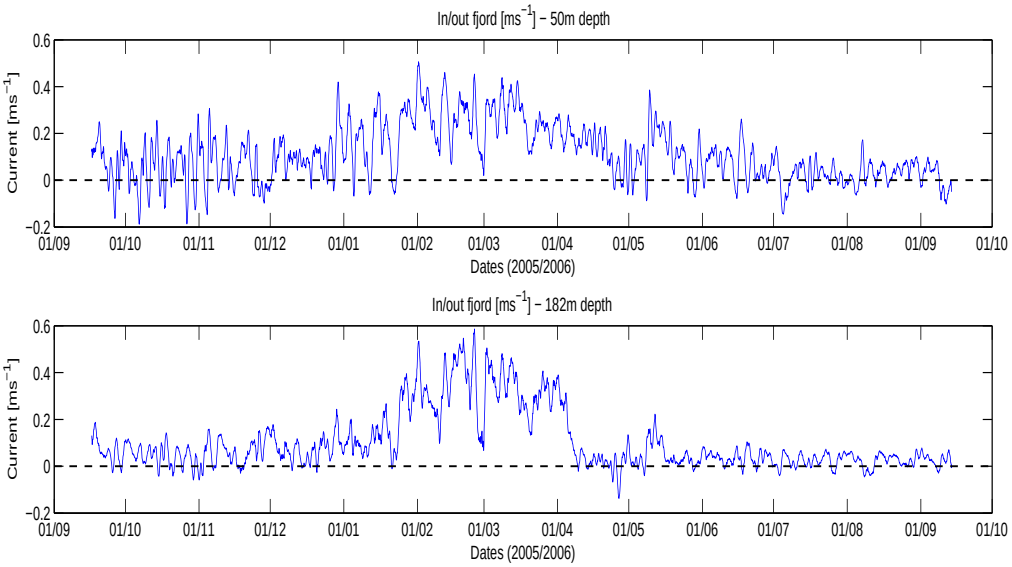

Figure 2.10: Current data from Mooring I [ms^{-1}] for two different depth, 50 m and 182 m. Positive values represent in-fjord current, while negative values represent an out-fjord current. The dashed line separates the in- and outflow.

Chapter 3

Theory and Methods

3.1 Governing parameters

The water column in the southern part of the Isfjorden Trough is found to be highly homogeneous, allowing us to apply a one layer model of the water column, neglecting density differences in the following calculations. Representative values for the relevant geophysical parameters in the study area around the Isfjorden Trough can be found in table 3.1.

The boundary current velocity V_{wsc}, representing the maximum velocity of the barotropic part of the WSC, is chosen to be between 0.20 ms^{-1} to 0.36 ms^{-1}. The length scale, L is the distance AW can penetrate the Isfjorden Trough from the position of the maximum current in the WSC. Horizontal and vertical eddy viscosities, A_h and A_v, are used to parameterise the turbulent fluxes in a fluid. The horizontal eddy is much larger than the vertical eddy as the ocean's motion is nearly always horizontal and the turbulent motion covers much longer distances in the horizontal than the vertical. The horizontal and vertical eddy viscosities are set to $A_h = 10\ \mathrm{m}^2\mathrm{s}^{-1}$ and $A_v = 0.01\ \mathrm{m}^2\mathrm{s}^{-1}$ respectively. These are typical values for the ocean and within the range of eddy viscosity values given in Pedlosky [1987]. The depth scale D is set to 500 m and represents the western boundary of the model setup where we find the maximum velocity of the WSC. The barotropic Rossby number, ε, which gives an indication of the importance of rotation varies with V_{wsc} and is in this case between 0.0175 and 0.0315. The eddy viscosities, Ekman numbers, Brunt-Väisälä frequency, stratification parameter and vertical e-folding scale are used to characterise the flow. The Rossby number, ε, and the Ekman numbers, E_h and E_v, have to be small for the lowest order flow to be geostrophic. Due to the small Ekman numbers, friction can be neglected, defining the flow as inviscid. The Brunt-Väisälä frequency, also called the buoyancy frequency, quantifies the static stability and is calculated in section 2.3.1. The frequency in Table 3.1 represents the seasonal extreme of stratification during summer and winter found by the CTD measurements. The Brunt-Väisälä frequency is also used to calculate the stratification parameter, $S^{\frac{1}{2}}$, and the e-folding scale, λ^{-1}, discussed in Section 2.3.1 and found in Table 2.2.

Table 3.1: Scales and scaling parameters appropriate for the West Spitsbergen Shelf and the Isfjorden Trough

V_{wsc}=0.20 - 0.36 ms^{-1}	Maximum WSC velocity (velocity scale)
L=80 km	Length scale
f=1.43 $\cdot 10^{-4}$ s^{-1}	Coriolis parameter
A_v = 0.01 m^2 s^{-1}	Vertical eddy viscosity
A_h = 10 m^2 s^{-1}	Horizontal eddy viscosity
D=500 m	Shelf break depth (depth scale)
$\varepsilon = \frac{V_{wsc}}{fL} = 0.0175$ to 0.0315	Barotropic Rossby number
$E_v = \frac{A_v}{fD^2}$	
$\frac{1}{2}E_v = 0.5\sqrt{E_v} = 8.37 \cdot 10^{-3}$	Vertical Ekman number
$E_h = \frac{0.5A_h}{fL^2} = 5.48 \cdot 10^{-6}$	Horizontal Ekman number
$N^2 = -\frac{g}{\rho}\frac{\partial \rho}{\partial z} = (3.5 \cdot 10^{-4})^2$ s^{-1} to $(7.8 \cdot 10^{-3})^2$ s^{-1}	Brunt-Väisälä frequency
$S^{\frac{1}{2}} = \frac{ND}{fL} =< 0.001$ to 0.342	Stratification parameter
$\lambda^{-1} = \frac{fL}{N} = \frac{D}{S^{1/2}} = 1500$ m to 32400 m	Vertical e-folding scale

3.2 Theory

The measurements and governing parameters lead us to a barotropic model assumption, describing the dynamics on the shelf west of Spitsbergen. Equations for describing the dynamics will be discussed with the basic theory from Pedlosky [1987], Chapter 3. Knowledge about the equation of motion, the vorticity equation and the theory of streamlines will give the reader an overall understanding of the model's functions.

The behaviour and the motion of the ocean can be described by the equation of motion, also known as the Navier-Stokes equation (3.1)

$$\frac{\partial \vec{v}}{\partial t} + \vec{v} \cdot \bigtriangledown \vec{v} = -f\vec{k} \times \vec{v} - \frac{1}{\rho} \bigtriangledown p - g\vec{k} + \bigtriangledown_A^2 \vec{v}, \tag{3.1}$$

where $\frac{\partial \vec{v}}{\partial t}$ and $\vec{v} \cdot \bigtriangledown \vec{v}$ are the local and advective acceleration respectively, $\bigtriangledown = \left(\frac{\partial}{\partial x}, \frac{\partial}{\partial y}, \frac{\partial}{\partial z}\right)$ and $\vec{v}$ = *(u,v,w)* are the eastward, northward and vertical current components. The Coriolis parameter is given by f and $\vec{k}$ is a unit vector along the z-axis, ρ is the density, p is the pressure, g is the gravity and the operator $\bigtriangledown_A^2$ is defined by

$$\bigtriangledown_A^2 = A^{(x)} \frac{\partial^2}{\partial x^2} + A^{(y)} \frac{\partial^2}{\partial y^2} + A^{(z)} \frac{\partial^2}{\partial z^2},$$

where A is the eddy viscosity in the x, y and z direction. Due to the small Ekman numbers, the eddy viscosity and friction will be neglected.

By looking at an incompressible fluid ($\frac{D\rho}{dt} = \frac{\partial \rho}{\partial t} + \vec{v} \cdot \bigtriangledown \rho = 0$) on the f-plane with no friction, and assuming the flow is homogeneous and barotropic, the shallow-water equation along the x-, y- and z-axis is given by

$$\frac{\partial u}{\partial t} + u\frac{\partial u}{\partial x} + v\frac{\partial u}{\partial y} - fv = -g\frac{\partial \eta}{\partial x}, \tag{3.2a}$$

$$\frac{\partial v}{\partial t} + u\frac{\partial v}{\partial x} + v\frac{\partial v}{\partial y} + fu = -g\frac{\partial \eta}{\partial y}, \tag{3.2b}$$

$$\frac{\partial w}{\partial t} = -g\frac{\partial \eta}{\partial z} = 0,$$

where η is the surface elevation calculated from the dynamical pressure being equal $p = \rho_0 g \eta$ and ρ_0 is a constant due to the Boussinesq approximation. By integrating the continuity equation

$$\frac{\partial u}{\partial x} + \frac{\partial v}{\partial y} + \frac{\partial w}{\partial z} = 0 \tag{3.3}$$

over the total depth H, the shallow water continuity equation is given by

$$\left(\frac{\partial u}{\partial x} + \frac{\partial v}{\partial y}\right) H + \frac{dH}{dt} = 0,$$

and if $H = D + \eta - h_B$, the continuity equation can be written as

$$\left(\frac{\partial u}{\partial x} + \frac{\partial v}{\partial y}\right) [D + \eta - h_B] + \frac{\partial \eta}{\partial t} + u\frac{\partial}{\partial x}(\eta - h_B) + \frac{\partial}{\partial y}(\eta - h_B). \tag{3.4}$$

The bottom variation is given by h_B with D as a characteristic reference depth (Figure 3.1).

Characteristic scales for the study area and dynamical parameters are defined with L as the length scale, T the time scale, V the velocity scale and N_0 the free-surface elevation. These scales are used to find the non-dimensional dependent and independent variables, denoted by primes:

$$(x, y) = L(x', y')$$

$$t = \frac{L}{V}t' = Tt'$$

$$(u, v) = V(u', v')$$

$$\eta = N_0\eta'$$

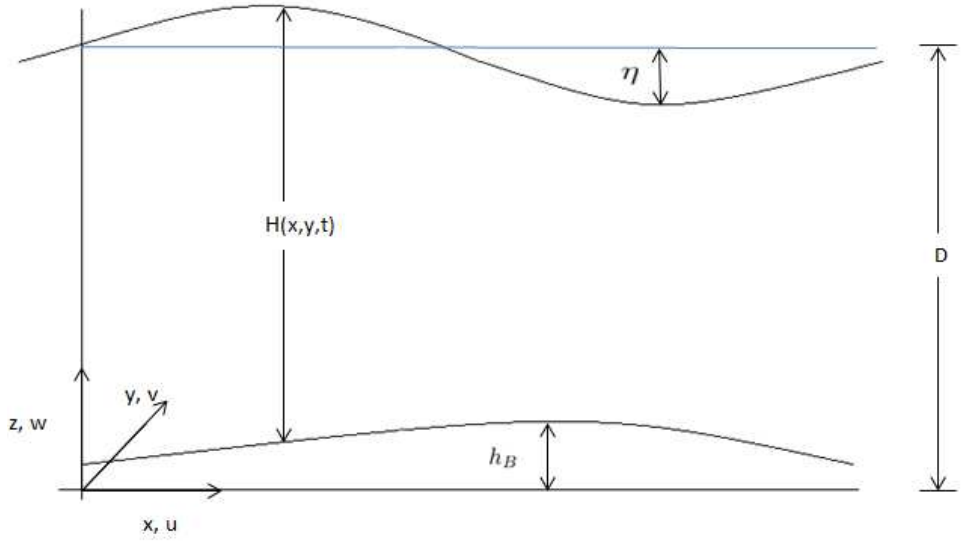

Figure 3.1: Schematic of the one layer model and boundary conditions, where η is the sea surface elevation, H is the total depth, h_B is the bottom variation and D is a reference depth.

The magnitude of the non-dimensional variables has to be of order unity. Characteristic scales should be chosen such that the length, time and velocity scales satisfy

$$\varepsilon = \frac{V}{fL} \ll 1, \tag{3.5a}$$

$$\varepsilon_T = \frac{1}{fT} \ll 1, \tag{3.5b}$$

where ε is the Rossby number and ε_T is the time dependent Rossby number for linear waves assumed to be equal to ε. Equations (3.2a), (3.2b) and (3.4) can now be written with non-dimensional variables

$$\frac{V}{T}\frac{\partial u'}{\partial t'} + \frac{V^2}{L}\left\{u'\frac{\partial u'}{\partial x'} + v'\frac{\partial u'}{\partial y'}\right\} - fVv' = -g\frac{N_0}{L}\frac{\partial \eta'}{\partial x'}, \tag{3.6a}$$

$$\frac{V}{T}\frac{\partial v'}{\partial t'} + \frac{V^2}{L}\left\{u'\frac{\partial v'}{\partial x'} + v'\frac{\partial v'}{\partial y'}\right\} + fVu' = -g\frac{N_0}{L}\frac{\partial \eta'}{\partial y'}, \tag{3.6b}$$

$$\frac{N_0}{T}\frac{\partial \eta^{'}}{\partial t^{'}} + \frac{V}{L}\left\{u^{'}\frac{\partial}{\partial x^{'}}(N_0\eta^{'} - h_B) + v^{'}\frac{\partial}{\partial y^{'}}(N_0\eta^{'} - h_B)\right\} + \frac{V}{L}\left[D + N_0\eta^{'} - h_B\right]\left[\frac{\partial u^{'}}{\partial x^{'}} + \frac{\partial v^{'}}{\partial y^{'}}\right] = 0. \tag{3.6c}$$

Equation (3.6) are simplified by choosing the parameter for free-surface elevation N_0 as

$$N_0 = \frac{fVL}{g} = \frac{V}{fL}\frac{f^2L^2}{g}. \tag{3.7}$$

By dividing the momentum equation (3.6a) and (3.6b) by fU and the mass-conservation equation (3.6c) by $\frac{V}{LD}$ and by using the equations for ε (3.5a), ε_T (3.5b) and N_0 (3.7), we arrive at three equations consisting of non-dimensional terms (the non-dimensional prime mark will in the following be omitted for simplicity), i.e.

$$\varepsilon_T\frac{\partial u}{\partial t} + \varepsilon\left\{u\frac{\partial u}{\partial x} + v\frac{\partial u}{\partial y}\right\} - v = \frac{\partial \eta}{\partial x}, \tag{3.8a}$$

$$\varepsilon_T\frac{\partial v}{\partial t} + \varepsilon\left\{u\frac{\partial v}{\partial x} + v\frac{\partial v}{\partial y}\right\} + u = \frac{\partial \eta}{\partial y}, \tag{3.8b}$$

$$\varepsilon_T F\frac{\partial \eta}{\partial t} + \varepsilon F\left\{u\frac{\partial \eta}{\partial x} + v\frac{\partial \eta}{\partial y}\right\} - u\frac{\partial}{\partial x}\left(\frac{h_B}{D}\right) - v\frac{\partial}{\partial y}\left(\frac{h_B}{D}\right) + \left\{1 + \varepsilon F\eta - \frac{h_B}{D}\right\}\left\{\frac{\partial u}{\partial x} + \frac{\partial v}{\partial y}\right\} = 0, \tag{3.8c}$$

where F is the influence of the surface elevation

$$F = \frac{f^2L^2}{gD} = \left(\frac{L}{R}\right)^2,$$

and R is the barotropic Rossby deformation radius and can be written as

$$R = \frac{(gD)^{\frac{1}{2}}}{f}.$$

Solutions of the non-dimensional momentum and mass-conservation equations (3.8) will be a function of x, y, z and ε. In this case we consider ε to be small, in order of unity or less, and u, v and η can therefore be written as an asymptotic series in ε.

$$u(x, y, z, \varepsilon) = u_0(x, y, z) + \varepsilon u_1(x, y, z) + \varepsilon^2 u_2(x, y, z) + ... \tag{3.9a}$$

$$v(x, y, z, \varepsilon) = v_0(x, y, z) + \varepsilon v_1(x, y, z) + \varepsilon^2 v_2(x, y, z) + ... \tag{3.9b}$$

$$\eta(x,y,z,\varepsilon) = \eta_0(x,y,z) + \varepsilon\eta_1(x,y,z) + \varepsilon^2\eta_2(x,y,z) + ... \tag{3.9c}$$

where u_0, v_0, η_0 *and* u_1, v_1, η_1 etc. are independent of ε. As shown earlier, $\varepsilon \ll 1$ and $\varepsilon_T \ll 1$, and (3.9) will be reduced to u_0, v_0 and η_0. A more complex flow is given by expansion to a higher order than only the first order. The O(1) from (3.8) yields

$$v_0 = \frac{\partial \eta_0}{\partial x}, \tag{3.10a}$$

$$u_0 = -\frac{\partial \eta_0}{\partial y} \tag{3.10b}$$

and

$$\frac{\partial u_0}{\partial x} + \frac{\partial v_0}{\partial y} = 0. \tag{3.11}$$

If $\frac{h_B}{D}$ is O(1) then by using (3.11), (3.8c) can be written as

$$u_0 \frac{\partial}{\partial x}\left(\frac{h_B}{D}\right) + v_0 \frac{\partial}{\partial y}\left(\frac{h_B}{D}\right) = 0 \tag{3.12}$$

or

$$\vec{v_0} \cdot \bigtriangledown \left(\frac{h_B}{D}\right) = 0,$$

which indicates the constraint that purely geostrophic motion must move along isobaths, preventing the flow from climbing up or down the bottom slope. This theory is an example of the Taylor-Proudman theorem placing a strong constraint on the flow saying that the vertical derivative of the horizontal velocity must be zero, hence there is no variation in the flow along the axis of rotation,

$$\frac{\partial u}{\partial z} = \frac{\partial v}{\partial z} = 0.$$

Further $\frac{h_B}{D}$ can be considered as

$$\frac{h_B}{D} = \varepsilon\eta_B(x,y), \tag{3.13}$$

where η_B, a new variable for the seafloor topography, is O(1). This gives a more interesting case, where the Rossby number is small, but large enough to break the constraint given by strict topographical steering in (3.12), i.e., that the motion is sufficiently distant from the exact geostrophic mode.

By inserting the asymptotic series of ε from (3.9) into the non-dimensional momentum and mass-conservation equations (3.8), the O(ε) terms in the shallow water equation yields

$$\frac{\partial u_0}{\partial t} + u_0\frac{\partial u_0}{\partial x} + v_0\frac{\partial u_0}{\partial y} - v_1 = -\frac{\partial \eta_1}{\partial x}, \tag{3.14a}$$

$$\frac{\partial v_0}{\partial t} + u_0\frac{\partial v_0}{\partial x} + v_0\frac{\partial v_0}{\partial y} + u_1 = -\frac{\partial \eta_1}{\partial y}, \tag{3.14b}$$

$$F\left\{\frac{\partial \eta_0}{\partial t} + u_0\frac{\partial \eta_0}{\partial x} + v_0\frac{\partial \eta_0}{\partial y}\right\} - u_0\frac{\partial \eta_B}{\partial x} - v_0\frac{\partial \eta_B}{\partial y} + \left(\frac{\partial u_1}{\partial x} + \frac{\partial v_1}{\partial y}\right) = 0. \tag{3.14c}$$

Now, u_1 and v_1 are ageostrophic velocities and $\eta_B = \frac{h_B}{\varepsilon D}$, where η_B is of O(1) and $\frac{h_B}{D}$ is of O(ε). If $\frac{h_B}{D}$ is much greater than O(ε), η_B has to be far greater than O(1) (see (3.13)), reducing the equation to the constraint that purely geostrophic motion must move along isobaths (3.12). By neglecting the pressure between (3.14a) and (3.14b) the time derivative of relative vorticity is found to be

$$\frac{d\zeta_0}{dt} = \frac{\partial \zeta_0}{\partial t} + u_0\frac{\partial \zeta_0}{\partial x} + v_0\frac{\partial \zeta_0}{\partial y} = -\left(\frac{\partial u_1}{\partial x} + \frac{\partial v_1}{\partial y}\right), \tag{3.15}$$

where the relative vorticity is defined as

$$\zeta_0 = \frac{\partial v}{\partial x} - \frac{\partial u}{\partial y}.$$

By using (3.10), the relative vorticity, ζ_0, can be written like

$$\zeta_0 = \frac{\partial v_0}{\partial x} - \frac{\partial u_0}{\partial y} = \frac{\partial}{\partial x}\frac{\partial \eta_0}{\partial x} - \frac{\partial}{\partial y}\frac{\partial \eta_0}{\partial y} = \bigtriangledown^2\eta_0, \tag{3.16}$$

where (3.14c) and (3.15) together give

$$\frac{d\zeta_0}{dt} = F\frac{d\eta_0}{dt} - \frac{d\eta_B}{dt}$$

or

$$\frac{d}{dt}\left\{\zeta_0 - F\eta_0 + \eta_B\right\} = 0. \tag{3.17}$$

The conservation statement (3.17) can be written in terms of η_0 by using (3.10) and (3.16)

$$\left[\frac{\partial}{\partial t} + \frac{\partial \eta_0}{\partial x}\frac{\partial}{\partial y} - \frac{\partial \eta_0}{\partial y}\frac{\partial}{\partial x}\right]\left[\bigtriangledown^2\eta_0 - F\eta_0 + \eta_B\right] = 0, \tag{3.18}$$

called the quasigeostrophic potential vorticity equation, in which all terms are evaluated through the use of their geostrophic values.

Since η_0 serves as a stream function for the O(1) velocity field, η_0 can be written as

$$\eta_0 = \psi(x, y, t),$$

in terms of which

$$u_0 = -\frac{\partial \psi}{\partial y},$$
$$v_0 = \frac{\partial \psi}{\partial x},$$

where ψ is the geostrophic stream function, or non-dimensional sea level. The direction of a fluid flow follows streamlines, which are isolines of the stream function. At an instant in time, every point on a velocity vector has a definite direction. The streamlines of the flow are the tangent to the direction field. Streamlines can make the flow easier to visualize and the streamlines can be plotted from the stream function. The volume flux between two different streamlines can be found by the difference between their corresponding values of the stream function [Kundu, 1990], and the volume flux stream functions, Ψ, can be written as the dimensional volume flux multiplied with the average depth between the streamlines as

$$\Psi = (\psi_2 - \psi_1) H_{mean} \cdot L \cdot V.$$

The non-dimensional quasigeostrophic potential vorticity equation (3.18) can then be rewritten in terms of the stream function

$$\left[\frac{\partial}{\partial t} + \frac{\partial \psi}{\partial x}\frac{\partial}{\partial y} - \frac{\partial \psi}{\partial y}\frac{\partial}{\partial x}\right]\left[\bigtriangledown^2 \psi - F\psi + \eta_B\right].$$

The non-dimensional potential vorticity can be written as

$$G(\psi) = \bigtriangledown^2 \psi - F\psi + \eta_B$$

where

$$\bigtriangledown^2 \psi + \eta_B = G(\psi) + F\psi = K(\psi), \tag{3.19}$$

where $K(\psi)$ is also an arbitrary function of ψ. The expression for potential vorticity $\bigtriangledown^2 \psi + \eta_B$ is valid only for small $\frac{h_B}{D}$. Equation (3.19) states that the sum of relative vorticity and potential vorticity is conserved along streamlines. Once $K(\psi)$ is determined for each streamline, (3.19) determines the steady flow. In order to find $K(\psi)$ it is necessary to specify $\bigtriangledown^2 \eta_0 + \eta_B$ at one point on each streamline.

3.3 Conservation of heat

The conservation of heat is given by

$$\rho c \frac{dT}{dt} = \rho c \left[\frac{\partial T}{\partial t} + \vec{v} \cdot \bigtriangledown T\right] = - \bigtriangledown \cdot \vec{\tau}, \tag{3.20}$$

where ρ is the density of the water, c is the heat capacity equal to 4000J kg^{-1}K^{-1}. The heat change with time is given as $\rho c\frac{dT}{dt}$, $\vec{v}$ is the velocity vector, T temperature and $\vec{\tau}$ is the heat flux. By adding the continuity equation (3.3), $\bigtriangledown \cdot \vec{v} = 0$, to the right hand side of (3.20), the conservation of heat is given by

$$\rho c\frac{dT}{dt} = \rho c\left[\frac{\partial T}{\partial t} + \bigtriangledown(\vec{v}T)\right] = -\bigtriangledown\vec{\tau}.$$

Reynolds' Transport Theorem gives an integration of volume

$$\int_V \rho c\frac{dT}{dt}dV = \rho c\int_V\left(\frac{\partial T}{\partial t} + \bigtriangledown(\vec{v}T)\right)dV = -\int_V \bigtriangledown\vec{\tau}dV.$$

No internal heat sources, $\frac{\partial T}{\partial t} = 0$, is assumed. Furthermore, by applying Gauss' law the heat equation is transformed to an area integral, giving

$$\rho c\int_A T\vec{v}\cdot\vec{n}\ dA = \int_A \vec{\tau}\cdot\vec{n}\ dA,$$

where $\vec{n}$ is the normal vector and A is the surface surrounding the volume. Here, we only consider heat flux to the atmosphere at the surface. Hence, by solving the integral on the left hand side and by writing the heat flux to the atmosphere as Q_a, the heat equation can be simplified to

$$\rho c(T_2v_2A_2 - T_1v_1A_1) = \int_A Q_a dA.$$

By assuming $v_1A_1 = v_2A_2 = \Psi$, where Ψ is the volume flux and A_0 is the surface area

$$\rho c\Psi(T_2 - T_1) = Q_A A_0,$$

$$dT = T_2 - T_1 = \frac{Q_A A_0}{\rho c\Psi}.$$

The dimensional volume flux, Ψ, can be calculated from the difference in streamlines multiplied by the average depth written as

$$\Psi = (\psi_2 - \psi_1)H_{mean}\cdot L\cdot V, \tag{3.21}$$

where H_{mean} is the mean value of the depth between ψ_1 and ψ_2. The conservation of heat and change in temperature following a streamline can then be written as

$$dT = \frac{Q_A A_0}{\rho c\Psi}. \tag{3.22}$$

Chapter 4

The Model

A one layer model made by Nilsen and Vaardal-Lunde [2012] using a finite-difference scheme was used to model the steady barotropic velocity field by numerically solving the quasigeostrophic potential vorticity equation on a f-plane. The boundary value problem can be formulated as a Poisson equation, written as an elliptic equation

$$\nabla^2\psi = \left(\frac{\partial^2\psi}{\partial x^2} + \frac{\partial^2\psi}{\partial y^2}\right) = \kappa(x, y) \tag{4.1}$$

where κ is a source term. By using a finite-difference scheme, the numerical solution of the Poisson equation (4.1) is given by

$$\frac{\psi_{j+1,k} - 2\psi_{j,k} + \psi_{j-1,k}}{\triangle^2} + \frac{\psi_{j,k+1} - 2\psi_{j,k} + \psi_{j,k-1}}{\triangle^2} = \kappa_{j,k}$$

or equivalent

$$\psi_{j+1,k} + \psi_{j-1,k} + \psi_{j,k+1} + \psi_{j,k-1} - 4\psi_{j,k} = \triangle^2\kappa_{j,k}$$

where j and k represent grid positions along the y- and x-axis and $\triangle = \triangle x = \triangle y$ is the grid spacing.

The bathymetry of the WSS and the coast of Spitsbergen used in the model is calculated (population mean) from a depth matrix based on the International Bathymetric Chart of the Arctic Ocean (IBCAO), from Jakobsson et al. [2008]. The resolution is chosen to be 4 km in a 73x35 (jxk) rectangular grid. Prins Karls Forland is later added to the bathymetry matrix by comparing the Forland strait and the area around Prins Karls Forland with a bathymetry map from the Norwegian Mapping Agency database, to get depth data as realistic as possible. The model is simplified by defining Prins Karls Forland as a peninsula, attached to the West Spitsbergen coastline, instead of an island. The northern part of the Forland strait is shallow, with the deepest part around 6 m and it is therefore assumed that the modification of Prins Karls Forland to a peninsula is a fair assumption. The y-axis of the model domain follows the 500 m isobath and indicates the seaward boundary, which in the model is stretched out into a

straight line. By making the 500 m isobath a straight line the coastline contour will be somewhat displaced. The model bathymetry is compared with the bathymetry map from IBCAO, seen in Figure 4.1. The grid indexing from the model are also shown in Figure 4.1, with a grid size of 4 km.

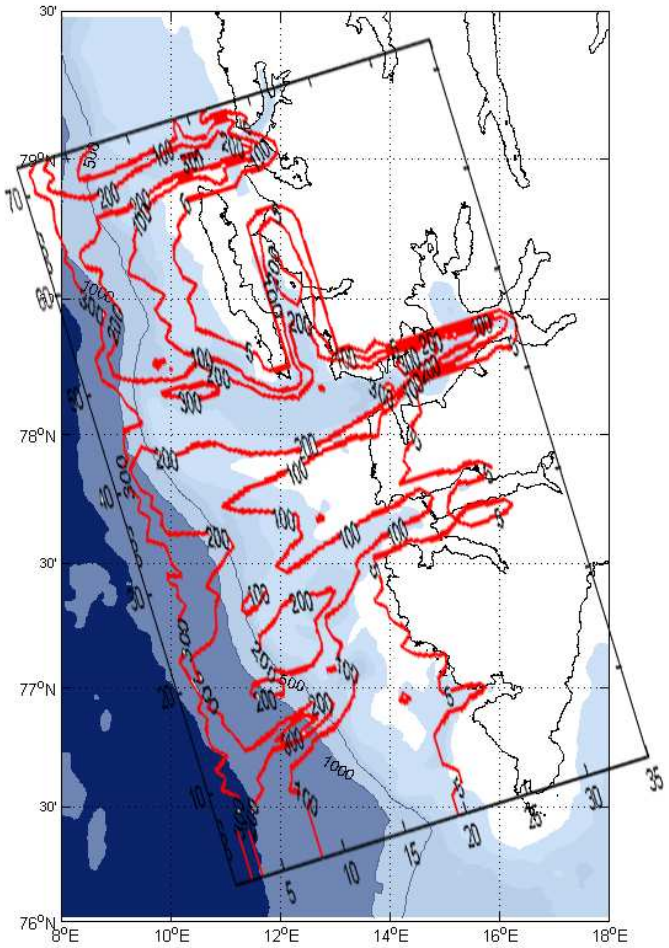

Figure 4.1: The depth contours of the model domain, in red lines marked with depth in [m], compared with a bathymetry map from IBCAO [Jakobsson et al., 2008]. The axis of the model domain is the grid indexes given in 4 km grid size. The 500 m and 1000 m isobaths are marked in the IBCAO map and the dark blue colour represents depths below 2000 m.

4.1 Boundary conditions

The relative vorticity at the upstream boundary is here assumed to be

$$\zeta = \frac{\partial v}{\partial x} = \frac{\partial^2 \psi}{\partial x^2},$$

indicating northward or southward current flow. The vorticity represents the change in current speed over a distance which varies during the seasons and years as seen in Figure 2.2. Boundary conditions need to be defined in order to find a solution. We choose no velocity normal to the coast, hence at the shore line, $x = L_x$, the stream function equals zero. At $x = 0$ the seaward streamline can be given as $\psi_0 = \zeta_0 \frac{L_x^2}{2V_{wsc}L} - \zeta_0 \frac{a}{V_{wsc}} \frac{L_x}{L} - \frac{L_x}{L}$. The streamline function are only allowed to be negative in order to be coupled to the WSC.

The geostrophic stream functions are given as a linear velocity profile and representing the WSC with origo over the 500 m isobath. The upstream boundary along the x-axis where $y = 0$, is written as

$$\frac{\partial^2 \psi_0}{\partial x^2} = -\zeta_0 \frac{L}{V_{wsc}}, \tag{4.2}$$

$$\frac{\partial \psi_0}{\partial x} = -\zeta_0 \frac{L}{V_{wsc}} \left(x - \frac{a}{L} \right) + 1,$$

$$\psi_0 = -\zeta_0 \frac{L}{2V_{wsc}} \left[x^2 - \left(\frac{L_x}{L} \right)^2 \right] + \left(\zeta_0 \frac{a}{V_{wsc}} + 1 \right) \left(x - \frac{L_x}{L} \right). \tag{4.3}$$

The distance from $x = 0$ to the boundary at the coast is given by L_x which equals 76 km at y=0. The length scale L is given from table 3.1 and a is the displacement of the WSC from the 500m isobath, in this case it equals zero. The velocity, V_{wsc}, is the chosen maximum velocity of the barotropic WSC. From (3.19) and (4.2) the Poisson equation now can be written as

$$-\zeta_0 \frac{L}{V_{wsc}} + \eta_B = K(\psi_{y=0}).$$

Using the source term $K(\psi) - \eta_B$ and grid spacing $\triangle^2$, the numerical solution is given by

$$-\frac{1}{4}\psi_{j-1,k} - \frac{1}{4}\psi_{j,k-1} + \psi_{j,k} - \frac{1}{4}\psi_{j+1,k} - \frac{1}{4}\psi_{j,k+1} = \frac{\triangle^2}{4} \left[-K(\psi_{j,k}) + \eta_{B_{j,k}} \right] \tag{4.4}$$

The result gives a square sparse coefficient matrix, derived from the second order elliptic equation

$$\psi_{j,k} A = \frac{\triangle^2}{4} \kappa(\psi), \tag{4.5}$$

where A is a matrix with a structure described as "tridiagonal with fingers" [Press et al., 2007], representing the equations for each grid point. Solution to (4.5) is found through Matlab's backslash command which is equivalent to a gaussian elemination. Initially, all values of ψ are set to zero except at the boundaries (j=1 and k=1). Along k=1, $\psi_{j,k}$ were computed according to (4.2), and then $\psi_{1,k}$ was set to $\psi_{1,1} = \psi_0(k)$ for all j to initialize the seaward boundary. For each successive iteration by Gaussian eliminations a new $\psi_{j,k}$ is calculated from (4.4) based on older values. Since $K(\psi)$ is conserved along streamlines (3.19) the function $K(\psi_{j,k})$ is determined by searching along the upstream boundary for the particular value in which $\psi_{j,k} = \psi_0(k)$ and

calculating $K(\psi) = -\zeta_0 \frac{L}{V_{wsc}} + \eta_B$ (j=1,k) at that point k. After each iteration a fractional change is calculated based on the old values and a solution is reached when the fractional change between the iterations converges towards a small value. In general, the solution converges after 5 iterations, but routinely a total of 15 iterations are performed.

4.1.1 Relative vorticity

By looking at Figure 2.2 it is seen that both the current velocity and the horizontal extent of the WSC varies from month to month over the years 2005/2006 and 2007/2008. The mean current velocity, representing a skew Gaussian profile fitted to the mean current data, from 2007/2008 and its corresponding relative vorticity is found in Figure 4.2, with data from Teigen et al. [2010].

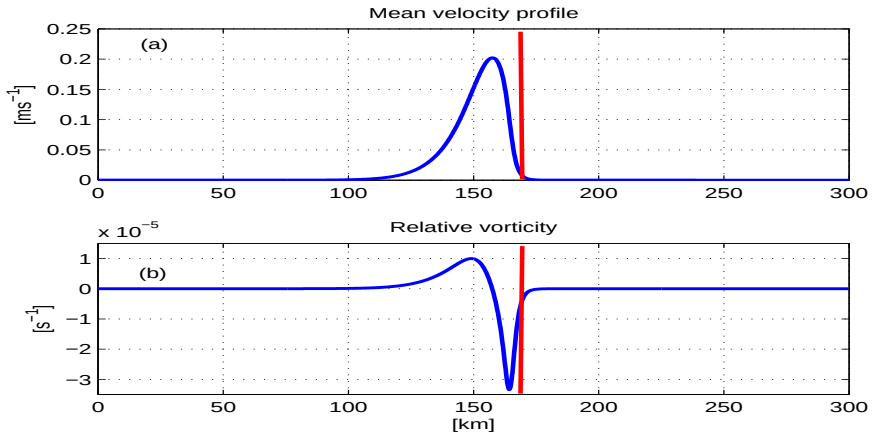

Figure 4.2: a) The skew Gaussian profile fitted to the mean current data from 2007/2008, b) The relative vorticity shows how the vorticity changes with the mean current profile. The red lines represent the region where the WSC can influence the transport of water on the slope and shelf region. The data is from Teigen et al. [2010], and the x-axis is explained in Teigen et al. [2010] Figure 1.

The current profile has its maximum velocity approximately over the 500 m isobath [Teigen et al., 2010]. The region where the WSC can influence the transport of water on the slope and shelf region is indicated by the red line which crosses the velocity profile (Figure 4.2a). At this point the corresponding relative vorticity is found, marked as a red line in Figure 4.2b. The relative vorticity in this region is equal to $\zeta = -0.4 \cdot 10^{-5}$ s^{-1}.

A constant relative vorticity of $\frac{\partial^2 \psi}{\partial x^2} = \zeta_0$, is used in the model. The calculated relative vorticity is found when the eastern part of the WSC profile is located just outside the Isfjorden Trough. The maximum velocity of the WSC is set to 0.20 ms^{-1}, representing the average velocity of the WSC found in Fahrbach et al. [2001]; Saloranta and Haugan [2004] and Teigen et al. [2010]. A chosen distance from the 500 m isobath to just outside the Isfjorden Trough, where the bathymetric contours of the trough approach the slope region, will represent a situation where

the WSC profile is not able to be topographically steered into the troughs and onto the WSS.

By using (4.3), the non-dimensional distance is found to be

$$x_{\psi_{0=0}} = 2\left(\frac{a}{L} + \frac{V_{wsc}}{\zeta_0 L}\right) - \frac{L_x}{L}, \tag{4.6}$$

where the dimensional relative vorticity is

$$\zeta_0 = \frac{2V_{wsc}}{xL - 2a + L_x}. \tag{4.7}$$

The distance from $x = 0$ to the Isfjorden Trough entrance can be written as $x = \alpha L$, where α is a constant equal to 0.1, making $x = \alpha\ L = 0.1\ L = 8000$ m, corresponding to where the Isfjorden Trough entrance is located. Assuming the velocity of the WSC is set to 0.20 ms^{-1}, the relative vorticity will be equal ζ_0 = -0.4762·10^{-5} s^{-1}. This constant relative vorticity, ζ_0, used in the model corresponds to the relative vorticity found in Figure 4.2b and is the relative vorticity that will lock the current to the continental slope so no leakage into the troughs and onto the shelf is possible, during a maximum WSC velocity of 0.20 ms^{-1}.

Chapter 5

Results

A one layer model is used to calculate the streamlines on the West Spitsbergen Shelf (WSS), i.e. the sea surface elevation, indicating the in- and outflow of WSC water in the troughs and WSS areas. The homogeneous water column during winter from the CTD measurements (Section 2.3.1) fulfils the requirement of a one layer model. At the shelf, the WSC is highly barotropic, and due to $\lambda^{-1} >> D$ (see Table 2.2), the barotopic assumption of the model is satisfied during winter time.

Figure 5.1 represents the sea surface elevation, where the light coloured area is the sea surface of different streamline values, plotted on top of the model bathymetry shown in brown colour. The non-dimensional streamline values are multiplied by one thousand to get a better picture of the spatial sea surface elevation. Since geostrophic currents in the northern hemisphere have higher pressure to the right, the sea surface tilt from the model indicates the direction and the volume transport of the current. Where the isobaths converge, so do the streamlines, indicating a stronger flow over steeper topography. The intensity of the barotropic branch of the WSC is highly seasonal with a stronger and broader flow during winter than summer, as shown in Figure 2.2 and discussed by Teigen et al. [2010]. Thus it is interesting to test the sensitivity of AW inflow, into the shelf troughs, to changes in the maximum velocity of the WSC in the model input.

A surface plot of the sea surface elevation from streamlines is shown in Figure 5.2, for an easier interpretation of the model results. Figure 5.2a shows the models topography where the Isfjorden Trough is indicated, while Figure 5.2b shows the exaggerated sea surface elevation with the direction of the corresponding current flow indicated. The sea surface elevation represents the elevation at the shelf break, corresponding to one and a half grid step towards the coast in the x-direction. The three arrows in Figure 5.2a and 5.2b mark the in- and outflow areas. We see that the Isfjorden Trough has an inflow on the southern side and a compensating outflow on the northern side, in agreement with the ADCP measurements from Figure 2.9.

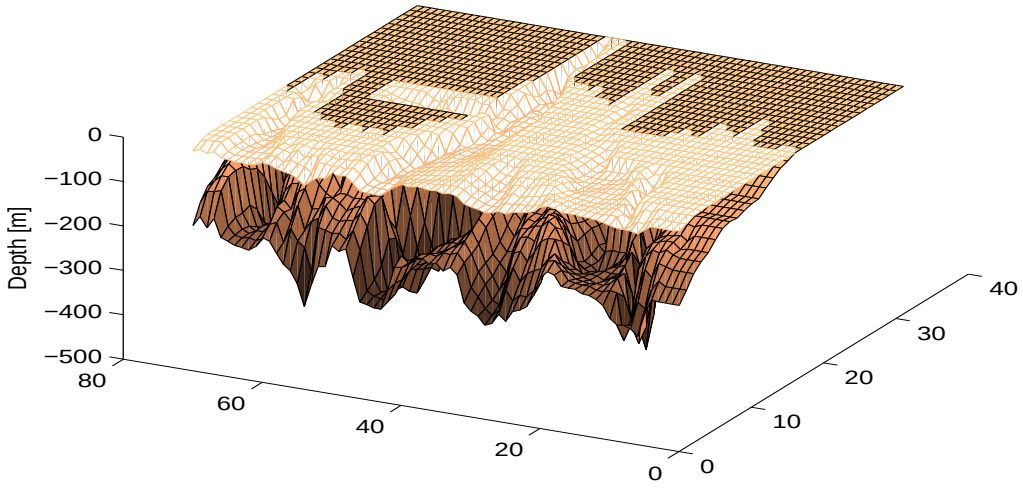

Figure 5.1: Streamlines showing the sea surface elevation i.e. the surface pressure. Light colour represents a mesh plot of the streamlines, multiplied by one thousand. The dark brown colour represents the bottom topography. The x- and y-axis are the k and j grid respectively with a resolution of 4 km, while the z-axis is the depth in [m]. Model input parameters are $V_{wsc} = 0.25$ ms^{-1} and $\zeta_0 = -0.4762 \cdot 10^{-5}$ s^{-1}.

5.1 Variations in the maximum velocity of the WSC

The maximum velocity of the WSC, hereafter only referred to as the velocity of the WSC, is assumed to be situated above the 500 m isobath. Moreover, we will keep the relative vorticity constant and study the effect of varying the velocity of the WSC, i.e. we will vary the velocity scale that represents the upstream boundary condition. From the boundary equations (4.3) and (4.6) it can be found that the terms deciding the sea surface elevation are the velocity of the WSC and the relative vorticity. The fraction $\frac{V_{wsc}}{\zeta_0 L}$ can give the same result if you increase V_{wsc} or decrease the magnitude of ζ_0, by keeping the other constant. From Table 5.1 the different velocities of the WSC that will be studied are shown, with equivalent change in relative vorticity. The equivalent relative vorticity would give the same result for (4.3) and (4.6) as increasing the WSC velocity from $V_{wsc} = 0.20$ ms^{-1}, which is the initial velocity of the WSC. The Rossby numbers for the different velocities are also presented in Table 5.1.

Figure 5.3 shows four different velocity profiles (straight lines) with the corresponding streamline profiles (curved lines) at the upstream boundary. The negative velocities of the WSC are neglected since the model concentrates only on the northward current flow. The streamline profiles are shown until the corresponding velocity reaches zero, but only the negative streamline values will be studied in this thesis. By choosing the velocity of the WSC to be 0.20 ms^{-1} it is seen from Figure 5.3 that the streamline profile (blue line) crosses zero at $x = 0.1$. The dimensional

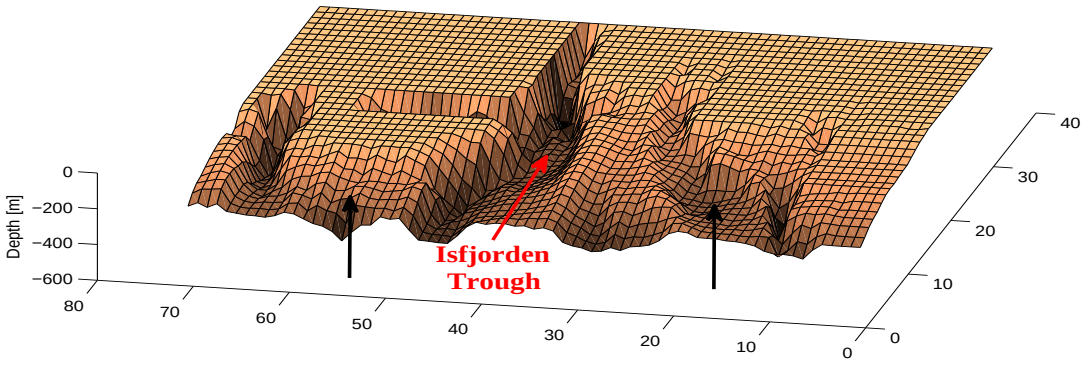

(a)

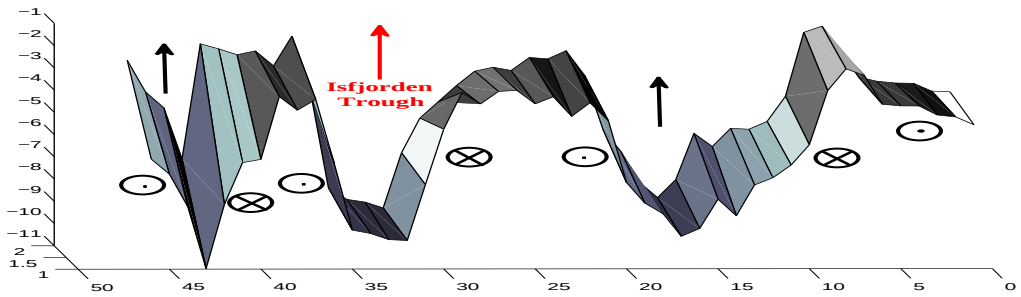

(b)

Figure 5.2: a) Bottom topography west of Spitsbergen. Isfjorden Trough and the small troughs north and south of the Isfjorden Trough are marked. b) Streamlines representing the exaggerated sea surface elevation at the shelf break, corresponding to one and a half grid steps towards the coast in the x-direction. The x- and y-axis are the k and j grid respectively with a resolution of 4 km. Circles with crosses indicate inflow, while circles with dots indicate outflow. Model input parameters are $V_{wsc} = 0.25$ ms^{-1} and $\zeta_0 = -0.4762 \cdot 10^{-5}$ s^{-1}.

value of $x = 0.1$ equals 8000 m, which is the distance from the y-axis to just outside the entrance of the Isfjorden Trough. Since the streamline that represents the sea surface pressure does not reach the Isfjorden Trough, inflow from the WSC is impossible. With an increase in the WSC velocity, the distance from the origo to where streamlines cross zero will increase (Figure 5.3) and an inflow into the Isfjorden Trough from the WSC can occur. The streamline values have lower negative numbers when the velocity of the WSC is increased. The last ocean grid point at the upstream boundary is found at $x = 0.9$, similar to grid point 18 that corresponds to a distance of 72 km from the origo towards the coast along the x-axis.

Table 5.1: Different velocities of the WSC and the equivalent relative vorticity for a constant velocity of 0.20 ms^{-1} are given in the Table. The non-dimensional Rossby numbers are also presented.

Velocity	**Equivalent rel.vorticity**	**Rossby number**
$V_{wsc} = 0.20\ ms^{-1}$	$\zeta_0 = -0.4762 \cdot 10^{-5}\ s^{-1}$	$\varepsilon = 0.0175$
$V_{wsc} = 0.21\ ms^{-1}$	$\zeta_0 = -0.4535 \cdot 10^{-5}\ s^{-1}$	$\varepsilon = 0.0184$
$V_{wsc} = 0.22\ ms^{-1}$	$\zeta_0 = -0.4329 \cdot 10^{-5}\ s^{-1}$	$\varepsilon = 0.0192$
$V_{wsc} = 0.23\ ms^{-1}$	$\zeta_0 = -0.4141 \cdot 10^{-5}\ s^{-1}$	$\varepsilon = 0.0202$
$V_{wsc} = 0.25\ ms^{-1}$	$\zeta_0 = -0.3810 \cdot 10^{-5}\ s^{-1}$	$\varepsilon = 0.0219$
$V_{wsc} = 0.28\ ms^{-1}$	$\zeta_0 = -0.3401 \cdot 10^{-5}\ s^{-1}$	$\varepsilon = 0.0245$
$V_{wsc} = 0.30\ ms^{-1}$	$\zeta_0 = -0.3175 \cdot 10^{-5}\ s^{-1}$	$\varepsilon = 0.0263$
$V_{wsc} = 0.34\ ms^{-1}$	$\zeta_0 = -0.2801 \cdot 10^{-5}\ s^{-1}$	$\varepsilon = 0.02979$
$V_{wsc} = 0.35\ ms^{-1}$	$\zeta_0 = -0.2721 \cdot 10^{-5}\ s^{-1}$	$\varepsilon = 0.0306$
$V_{wsc} = 0.36\ ms^{-1}$	$\zeta_0 = -0.2646 \cdot 10^{-5}\ s^{-1}$	$\varepsilon = 0.0315$

5.1.1 The velocity of the WSC equals 0.20 ms^{-1}

When the velocity of the WSC equals 0.20 ms^{-1}, the flow is topographically steered along the shelf slope with no flow entering into the troughs (Figure 5.4). The flow is a jet-like current confined over the steeper continental slope.

5.1.2 The velocity of the WSC equals 0.21 ms^{-1}

By increasing the velocity of the WSC by merely 0.01 ms^{-1}, to 0.21 ms^{-1}, an inflow of water into the Isfjorden Trough directly from the WSC can be seen (Figure 5.5a). The streamlines mainly follows the 200 m isobath or deeper areas and increases from -119 m^2s^{-1} in the northern part of the trough entrance to 0 m^2s^{-1} just above the 200 m isobath. The $\psi = 0$ streamline can be found in both the northern and southern part of the trough, where no current exists. The difference between -119 m^2s^{-1} and 0 m^2s^{-1} represents the tilt of the surface giving a pressure gradient, with higher pressure towards shallower areas and lower pressure at the location of the minimum streamline value. The pressure gradient represents the in- and outflow from the trough, on the southern and northern sides respectively. The distance from the minimum streamline to the zero streamline is longer on the southern side than on the northern side, indicating higher current speed in the northern part of the trough, while the southern part has a larger inflow area. The

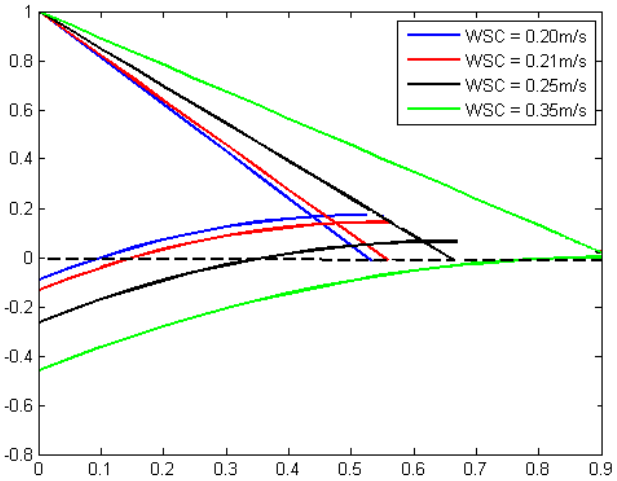

Figure 5.3: Velocity profiles at the upstream boundary of the model, y=0, with a constant relative vorticity. The velocity of the WSC shown are 0.20 ms^{-1}, 0.21 ms^{-1}, 0.25 ms^{-1} and 0.35 ms^{-1}. The x-axis is given in non-dimensional distance from x=0 towards the shelf, while the y-axis is given in non-dimensional current velocity overlying the 500 m isobath. The dashed line represents where the streamlines cross zero.

larger current speed in the northern part of the trough is also seen in Figure 5.5b representing the calculated current vectors from the model by blue arrows.

The current found in the Kongsfjorden Trough is water from two different locations. One branch of water flows from the Isfjorden Trough and northward along the 200 m isobath before it enters the Kongsfjorden Trough. Another branch of water flowing into the Kongsfjorden Trough is water that has been in contact with the WSC in the southern part of the small trough west of Forlandsbanken. This branch of water follows close to the 200 m isobath, parallel to the water from the Isfjorden Trough, and enters the Kongsfjorden Trough in its middle part.

5.1.3 The velocity of the WSC from 0.22 ms^{-1} to 0.23 ms^{-1}

By increasing the velocity of the WSC from 0.21 ms^{-1} to 0.22 ms^{-1}, the streamlines cross the 200 m isobath along the shelf of Spitsbergen. With an increase of the WSC velocity to 0.23 ms^{-1} cause the streamlines to move closer to the 100 m isobath, along the shelf of Spitsbergen. Figure 5.6 shows a pronounced change in the topographically steered flow from the two velocities, V_{wsc} = 0.22 ms^{-1} and 0.23 ms^{-1}, where the stronger velocity causes more water from the WSC to enter shallower areas on the shelf. The value of the minimum streamline varies from -147 m^2s^{-1} when the velocity of the WSC equals 0.22 ms^{-1} to -174 m^2s^{-1} when the velocity of the WSC is set to 0.23 ms^{-1}; both cases are found in the northern part of the Isfjorden Trough (Figure 5.6a and 5.6c). The inflow into the Isfjorden Trough during a WSC velocity of 0.22 ms^{-1}, follows the southern slope area close to the 200 m isobath where the shelf area shallower than 200 m is not

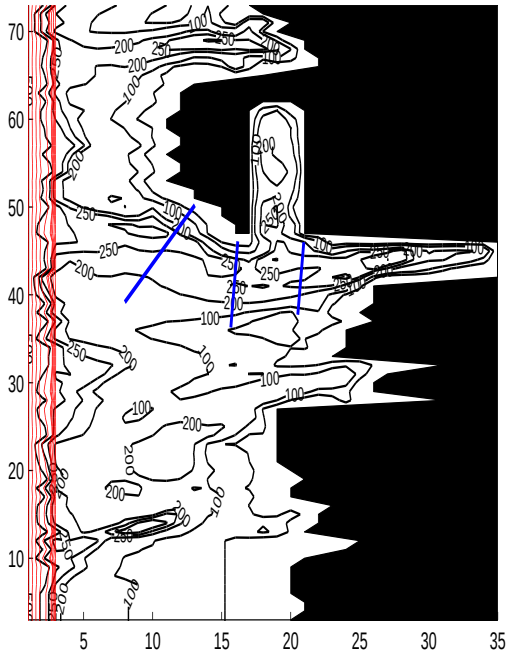

Figure 5.4: A jet-like current confined over the steeper continental slope (red lines represent streamlines) with no flow entering the troughs. Black contours represent the model bathymetry in [m]. The input parameter for the WSC is $V_{wsc} = 0.20$ ms^{-1}. The x- and y-axis are the k and j grid respectively with a resolution of 4 km.

much affected by the WSC. While looking at the inflow during a WSC velocity of 0.23 ms^{-1}, the shelf area is much more affected by the WSC, where streamlines can be found over large area between the 200 m and 100 m isobaths (Figure 5.6c). For both of these WSC velocities, one branch of water entering the Isfjorden Trough is derived directly from the WSC, while another branch is originating from the shallower shelf areas south of the trough. Water that has been recirculating Bredjupet (see Figure 2.3) is now transported northwards on the shelf, entering the Isfjorden Trough from the south. Calculated current vectors from the model (Figures 5.6b and 5.6d) indicate the in- and outflow areas.

The Kongsfjorden Trough still has inflow from two different branches of water as discussed in Section 5.1.2. When shifting the maximum velocity of the WSC from 0.22 ms^{-1} to 0.23 ms^{-1}, more inflow from the WSC is also found in Bredjupet and towards Bellsund.

5.1.4 The velocity of the WSC from 0.25 ms^{-1} to 0.34 ms^{-1}

Figure 5.7 shows streamlines for different velocities of the WSC, being 0.25 ms^{-1}, 0.28 ms^{-1}, 0.30 ms^{-1} and 0.34 ms^{-1}. The streamlines for a WSC velocity of 0.25 ms^{-1} (Figure 5.7a) shows a similar pattern as for a WSC velocity of 0.23 ms^{-1} (Figure 5.6c). A stronger flow

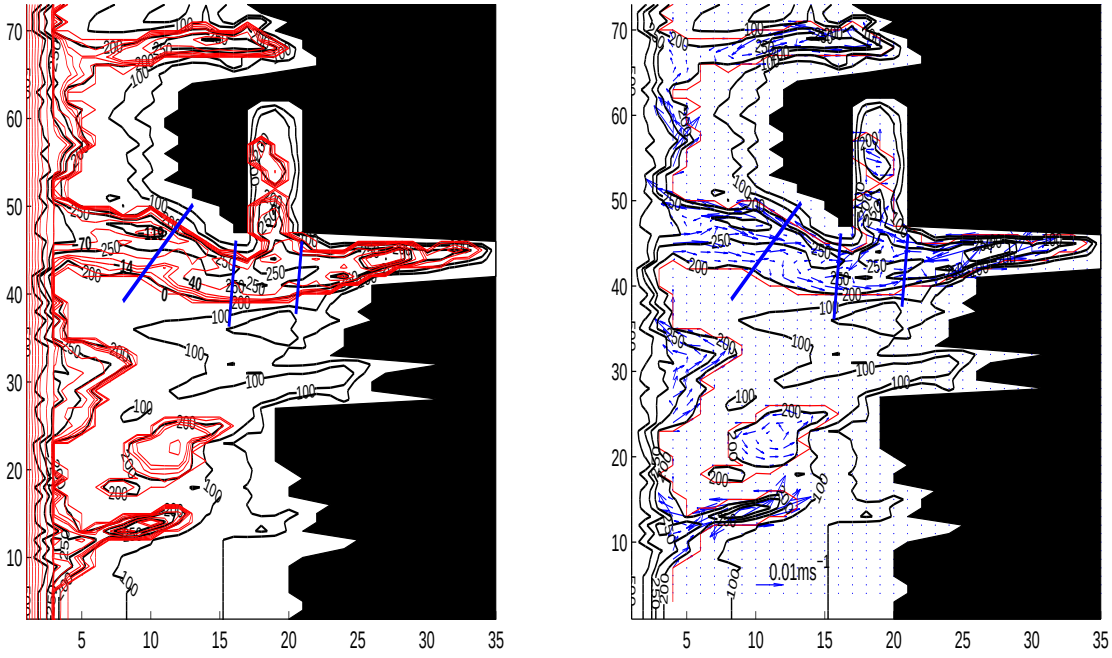

(a) (b)

Figure 5.5: a) Streamlines [m^2s^{-1}] in red with $V_{wsc} = 0.21$ ms^{-1} and calculated current vectors shown in b), as blue arrows. The red line in b) represents a streamline contour close to zero and the black lines represent the isobaths [m]. Blue lines represent the ADCP sections (discussed in Section 2.3.2) and the x- and y-axis are the k and j grid respectively with a resolution of 4 km.

can be found towards Bellsund and the WSC inflow also covers shallower areas along the shelf west of Spitsbergen. The minimum streamline in the Isfjorden Trough has a lower value than earlier (-223 m^2s^{-1}), indicating a larger sea surface elevation. Increasing the current from 0.25 ms^{-1} to 0.28 ms^{-1} (Figure 5.7b), lets the flow enter shallower isobaths than seen for a WSC velocity of 0.25 ms^{-1} (Figure 5.7a). The minimum streamline value in the Isfjorden Trough is now - 274 m^2s^{-1}, showing the same inflow pattern as earlier. The flow along the shelf from the Isfjorden Trough and the flow from the small trough west of Forlandsbanken are still found flowing into the Kongsfjorden Trough. But now a new branch of inflow is observed; an inflow of water directly in contact with the WSC is found in the southern part of the Kongsfjorden Trough entrance, following the 200 m isobath parallel to the water that has been circulating the small trough west of Forlandsbanken. Using a WSC velocity of 0.30 ms^{-1} (Figure 5.7c), giving a minimum streamline value of - 278 m^2s^{-1}, does not change the pattern of the flow much from a WSC velocity of 0.28 ms^{-1} (Figure 5.7b). Increasing the velocity of the WSC from 0.30 ms^{-1} to 0.34 ms^{-1} (Figure 5.7d), streamlines cross the 50 m isobath and approaches the coast. The minimum streamline value is now found to be - 294 m^2s^{-1}. A third branch of inflowing water is

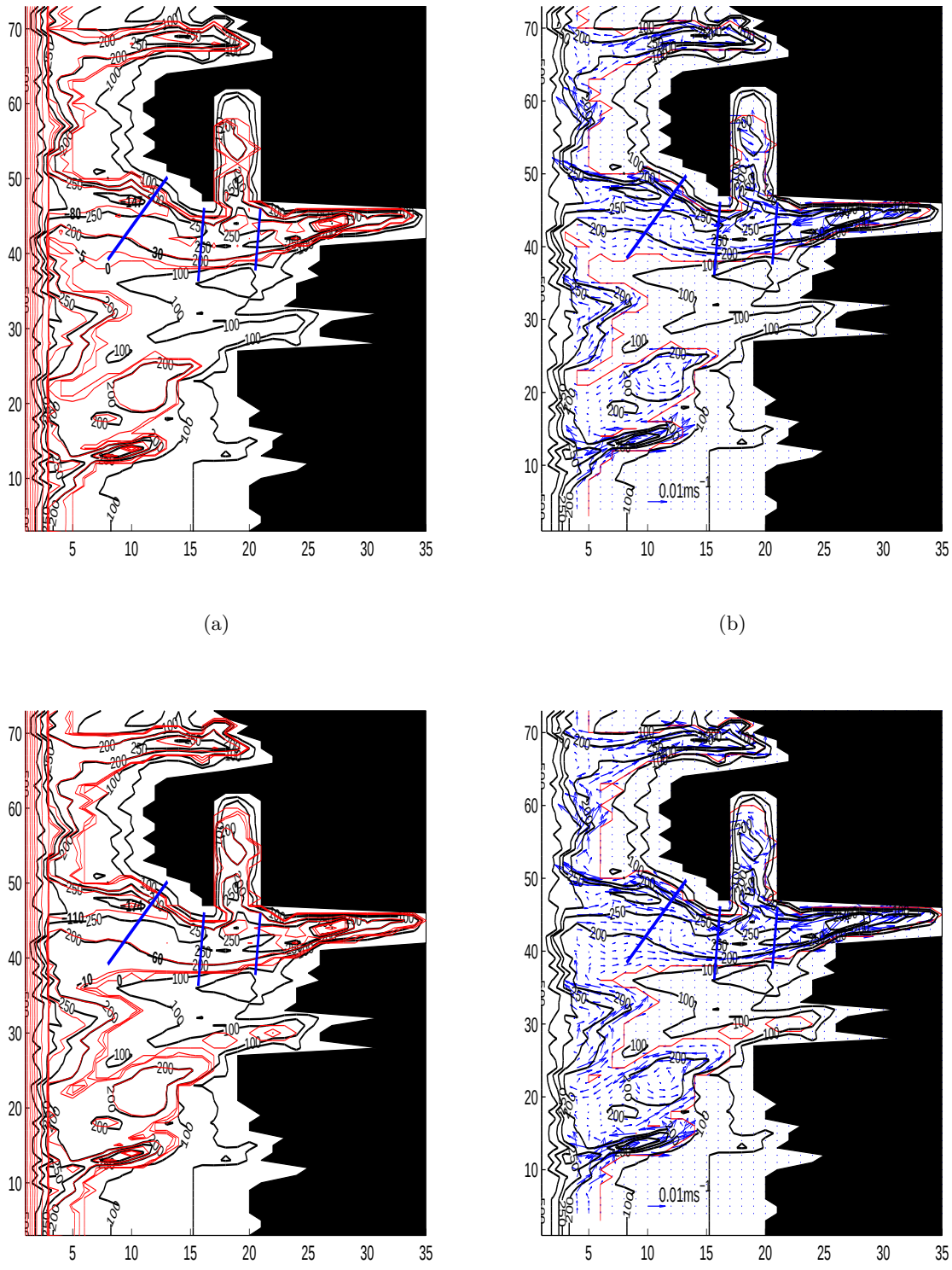

(a) (b)

(c) (d)

Figure 5.6: Same as Figure 5.5, but the streamlines are given for a WSC velocity of a) 0.22 ms^{-1} with current vectors shown in b) and a WSC velocity of c) 0.23 ms^{-1} with current vectors shown in d).

now observed in the Isfjorden Trough, following the coast from the upstream boundary. The flow into the Kongsfjorden Trough is now only from the branch of water coming from the Isfjorden Trough following the shelf northward and entering the Kongsfjorden Trough between the 200 m and 50 m isobaths. The flow in the small trough west of Forlandsbanken is re-circulated at the 250 m isobath before it follows the WSC northward. Also, the direct connection between the Kongsfjorden Trough and the WSC has disappeared.

5.1.5 The velocity of the WSC from 0.35 ms^{-1} to 0.36 ms^{-1}

By increasing the WSC velocity to 0.35 ms^{-1}, streamlines indicate flow all the way towards the coast (Figure 5.8a). The flow is in this case very similar to what is observed during a WSC velocity of 0.34 ms^{-1} (Figure 5.7d), but now has a minimum streamline value of -310 m^2s^{-1} in the Isfjorden Trough. Due to some closed streamline cells in the Isfjorden Trough, interpreted as local circulation, the streamline value of -310 m^2s^{-1} is not a representative measure of the in- and outflow of the Isfjorden Trough. Southward current vectors (Figure 5.8b) are observed, mostly in the outer part of the trough's entrance.

If we set the WSC velocity to 0.36 ms^{-1} the inflow picture changes (Figures 5.8c and 5.8d). The streamline profile from Figure 5.3 will in this case cross the zero line at 75 km, which at the upstream boundary will be the coast. The current vectors (Figure 5.8d) are now at the upstream boundary only found close to the y-axis and not on the shelf. Further north on the shelf the velocity vectors still represent a flow on the shelf area with a southward transport several places. The flow is in this case more chaotic as the streamlines are not just following isobaths but cross them at several places. The model setup now represents more of a coastal current, than a direct inflow effect of the WSC.

5.2 Volume transport

The volume transport of the flow entering and leaving the Isfjorden Trough is calculated from (3.21), found in Section 3.3. The volume transport will be calculated over a cross section close to the ADCP and CTD section 2 (see the red line in Figure 5.9). The cross section represents an area, south of Prins Karls Forland, where in- and outflow occur over a distance of 52 km.
The in-, out- and net flow is calculated in Table 5.2, showing how the volume transport varies for different velocities of the WSC. The variation of the net volume transport will be discussed in Chapter 6. Figure 5.10 represents the volume transport for the WSC velocities a) 0.21 ms^{-1}, b) 0.22 ms^{-1}, c) 0.23 ms^{-1}, d) 0.24 ms^{-1}, e) 0.25 ms^{-1} and f) 0.30 ms^{-1}. Larger values of the WSC velocity are not included because the pattern of the volume transport looks similar for velocities between 0.30 ms^{-1} and 0.35 ms^{-1}. The volume transport is plotted on top of isobaths to identify over which isobaths the in- and outflow take place in the Isfjorden Trough. An inflow in the southern part and an outflow in the northern part is seen during all the WSC velocities used in Figure 5.10. By increasing the WSC velocity from 0.21 ms^{-1} to 0.30 ms^{-1} the maximum

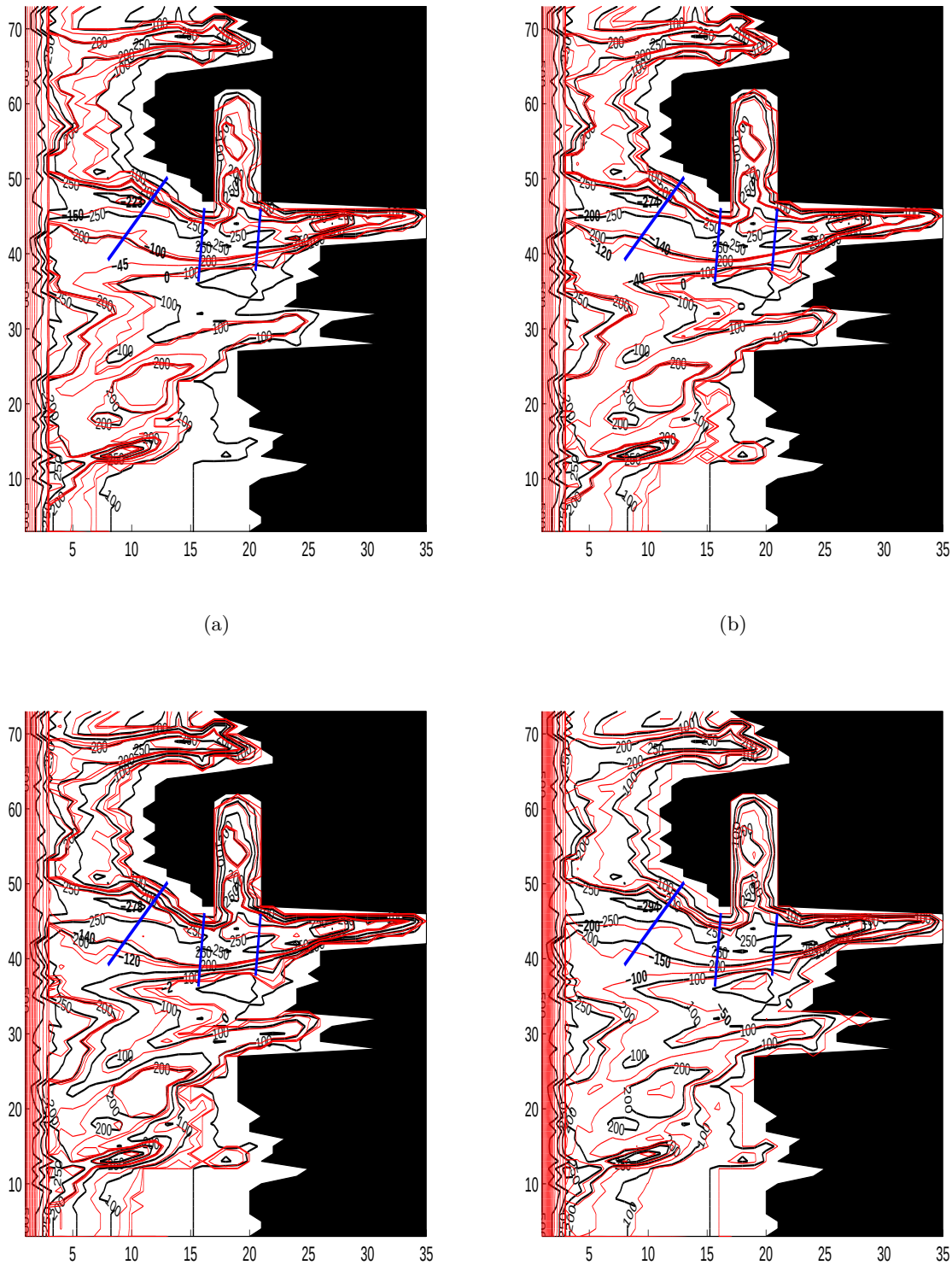

(a) (b)

(c) (d)

Figure 5.7: Same as Figure 5.5, but the streamlines are given for a WSC velocity of a) 0.25 ms^{-1} b) 0.28 ms^{-1} c) 0.30 ms^{-1} and d) 0.34 ms^{-1}.

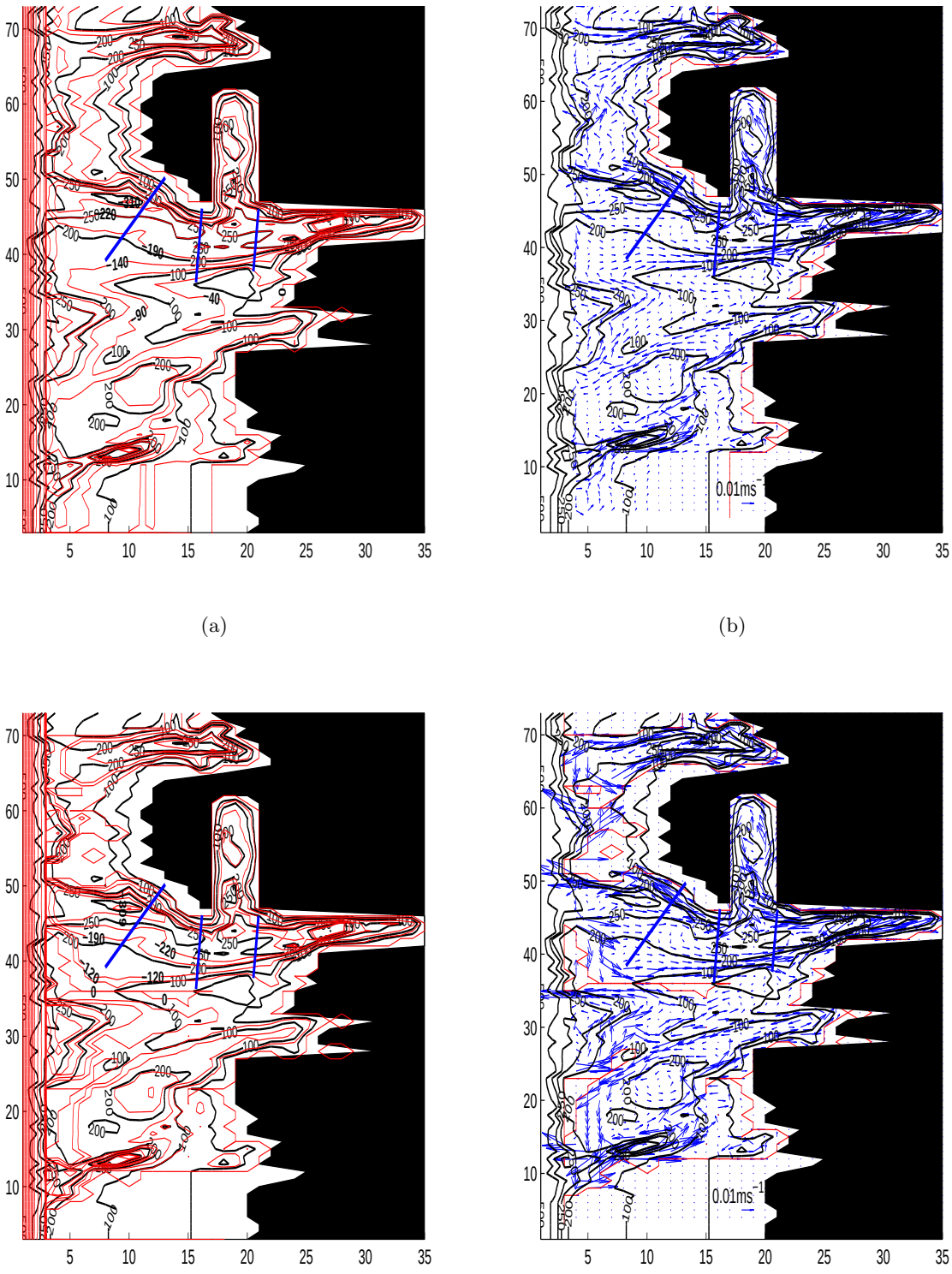

(a) (b)

(c) (d)

Figure 5.8: Same as Figure 5.5, but the streamlines are given for a WSC velocity of a) 0.35 ms^{-1} with current vectors shown in b) and a WSC velocity of c) 0.36 ms^{-1} with current vectors shown in d).

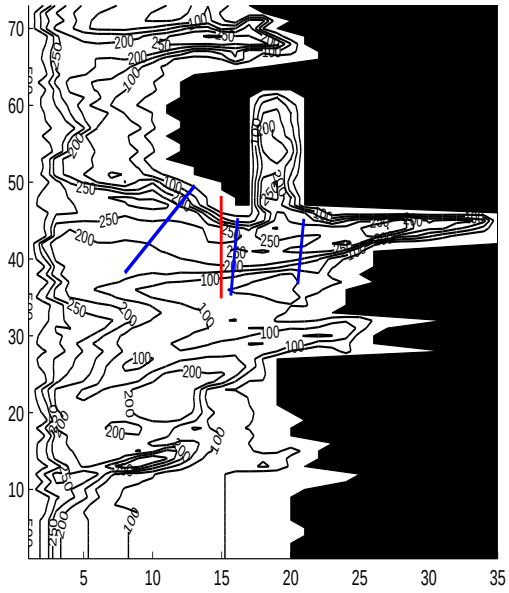

Figure 5.9: Depth contours from the model where the red line represents the area of where the volume transport will be calculated (from y=35 to y=48 at x=15). The axis ticks represent the model grid. Depth contours are shown as black lines in [m] and the blue lines indicate the ADCP sections discussed in Section 2.3.2.

volume transport in the trough is drawn towards steeper topography. Outflow from the trough has two peaks of transport during a WSC velocity of 0.21 ms^{-1} and 0.22 ms^{-1}, both around the 250 m isobath. The southern peak of outward transport reverses and becomes an inflowing source when increasing the WSC velocity to 0.23 ms^{-1} or more, leading to two peaks of inflow when the WSC velocity equals 0.23 ms^{-1} or more. The maximum outward transport is always located at grid point 44 with its maximum value during a WSC velocity of 0.34 ms^{-1}, seen in Table 5.2. From Table 5.2 the maximum inflow is also found for this WSC velocity. Between the 200 m and 250 m isobaths, at grid point 41, only a minor flow is observed, being close to zero through all the considered velocities of the WSC (Figure 5.10).

Figure 5.11 shows three cross sections in the Isfjorden Trough where the volume transport is calculated for a WSC velocity equal to 0.25 ms^{-1}, in order to look into how the current moves along isobaths. The maximum volume transport into the trough in the outer section is found approximately over the 250 m isobath, while a smaller inflow is found over a slightly shallower area. In the middle section, the maximum inflow is concentrated between the 100 m and 150 m isobaths, with a smaller inflow found at the 250 m isobath. The inner section shows a maximum inflow over the 200 m isobath, with a smaller inflow over the 250 m isobath. While the maximum inflow in section 2 is found between the 100 m to 150 m isobaths, the maximum inflow in section 3 is found over the 200 m isobath, indicating that the inflow moves towards greater depths from

the middle section to the inner section of the Isfjorden Trough. Three peaks of outflow can be found in the inner section, where outflow found in the northern part is located over the 200 m isobath, while the maximum outflow is located over the greatest depth. The middle section has the maximum outflow over the 250 m isobath, while the outer section has the maximum outflow over the 300 m isobath.

Table 5.2: The in-, out- and net volume transport for different velocities of the WSC. The volume transport is calculated for the section south of Prins Karls Forland (red line in Figure 5.9). The positive values indicating inflow, are added together in Ψ_{in}, while the negative values indicating outflow, are added together and represented by Ψ_{out}. The net flow, Ψ_{net}, is the sum of Ψ_{in} and Ψ_{out}.

Velocity	**Volume transport** [m^3s^{-1}]		
$V_{wsc} = 0.20$ ms^{-1}	$\Psi_{in} = 0$	$\Psi_{out} = 0$	$\Psi_{net} = 0$
$V_{wsc} = 0.21$ ms^{-1}	$\Psi_{in} = 13635$	$\Psi_{out} = -12861$	$\Psi_{net} = 774$
$V_{wsc} = 0.22$ ms^{-1}	$\Psi_{in} = 18386$	$\Psi_{out} = -18310$	$\Psi_{net} = 76$
$V_{wsc} = 0.23$ ms^{-1}	$\Psi_{in} = 19408$	$\Psi_{out} = -20077$	$\Psi_{net} = -670$
$V_{wsc} = 0.24$ ms^{-1}	$\Psi_{in} = 25246$	$\Psi_{out} = -26067$	$\Psi_{net} = -822$
$V_{wsc} = 0.25$ ms^{-1}	$\Psi_{in} = 28346$	$\Psi_{out} = -28469$	$\Psi_{net} = -123$
$V_{wsc} = 0.28$ ms^{-1}	$\Psi_{in} = 34551$	$\Psi_{out} = -33854$	$\Psi_{net} = 670$
$V_{wsc} = 0.30$ ms^{-1}	$\Psi_{in} = 34691$	$\Psi_{out} = -33957$	$\Psi_{net} = 734$
$V_{wsc} = 0.34$ ms^{-1}	$\Psi_{in} = 36645$	$\Psi_{out} = -37290$	$\Psi_{net} = -644$
$V_{wsc} = 0.35$ ms^{-1}	$\Psi_{in} = 33267$	$\Psi_{out} = -34810$	$\Psi_{net} = -1543$
$V_{wsc} = 0.36$ ms^{-1}	$\Psi_{in} = 33267$	$\Psi_{out} = -37453$	$\Psi_{net} = 1682$

5.3 Heat loss

The heat loss to the atmosphere for a certain area can be derived from the conservation of heat (3.22) in Section 3.3, knowing the heat flux to the atmosphere. By choosing the winter time as a case study with $V_{wsc} = 0.25$ ms^{-1} and $\zeta_0 = -0.4762 \cdot 10^{-5}$ s^{-1}, the shaded area in Figure 5.12 is the inflow area where the heat loss is calculated, referred to as A_0 in (3.22). The shaded area A_0 equals 192 km^2 and is calculated from $6 \triangle x \cdot 2 \triangle y$ (from x=15 to x=21 and from y=38 to y=40). The volume flux is calculated from (3.21) representing the volume transport between y=38 and y=40 at $x = 15$. The volume transport is $2.25 \cdot 10^4$ m^3s^{-1} corresponding to 0.025 Sv (1 Sv = $10^6 m^3s^{-1}$) and is assumed to be constant within the shaded area in Figure 5.12.

The heat flux to the atmosphere varies both seasonally and interanually. Teigen [2011] estimated that the heat loss can reach a maximum of -500 Wm^{-2} in winter. During 2007/2008 and 2008/2009 the average winter net surface heat flux along the WSS reached -260 Wm^{-2} and -220 Wm^{-2}, respectively [Teigen, 2011], where the negative heat flux implies a heat loss from the

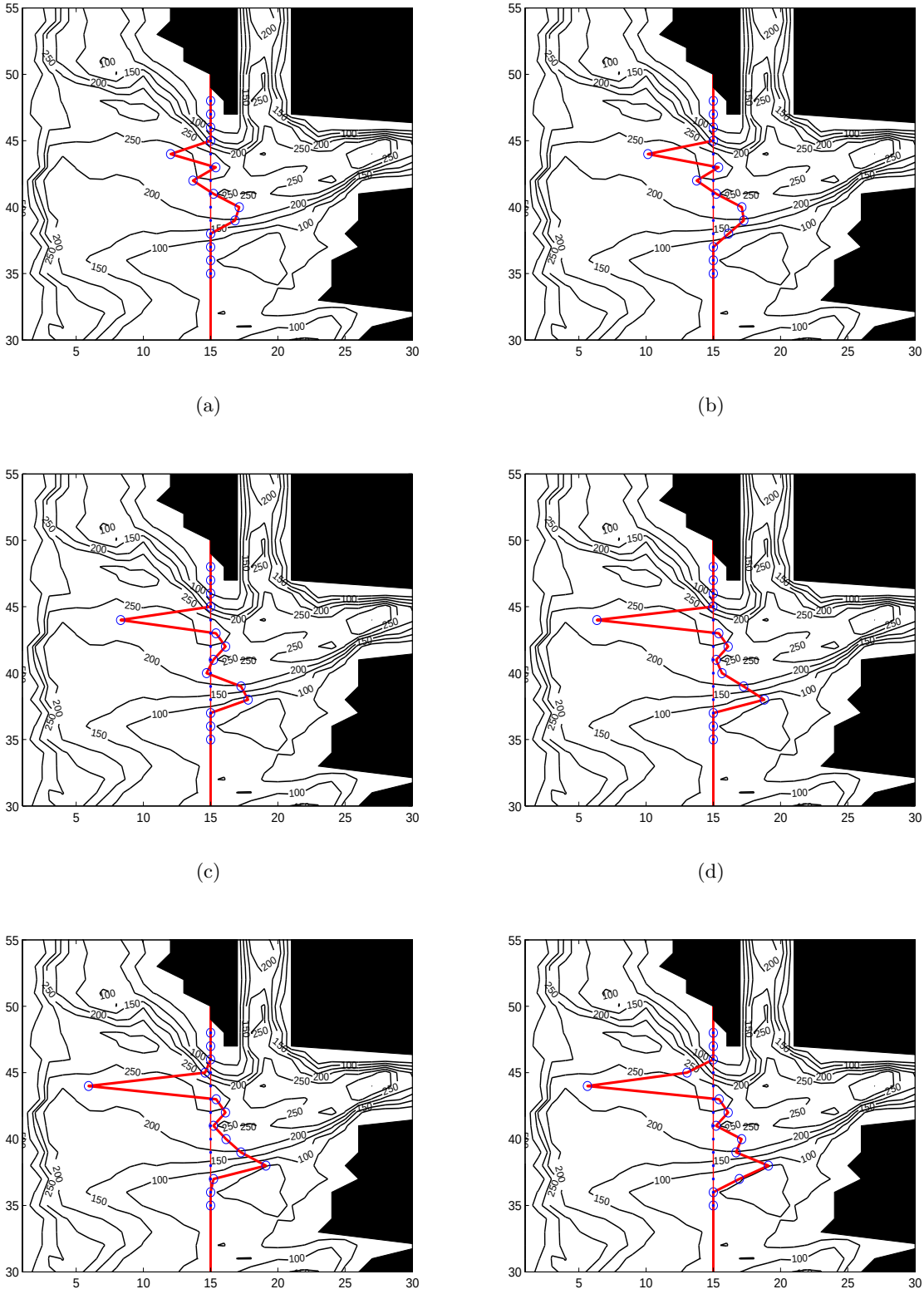

(a) (b)

(c) (d)

(e) (f)

Figure 5.10: Volume transport for the marked red line in Figure 5.9. The thin red line represents the zero line where flow to the left of the line indicates outflow and the flow to the right of the line indicates inflow. The bold red line represents the volume transport. The blue dots on the zero line at $x = 15$ indicate the position where the volume transport, shown with blue circles, occurs. The different velocities used for the WSC are a) 0.21 ms^{-1} b) 0.22 ms^{-1} c) 0.23 ms^{-1} d) 0.24 ms^{-1} e) 0.25 ms^{-1} f) 0.30 ms^{-1}.

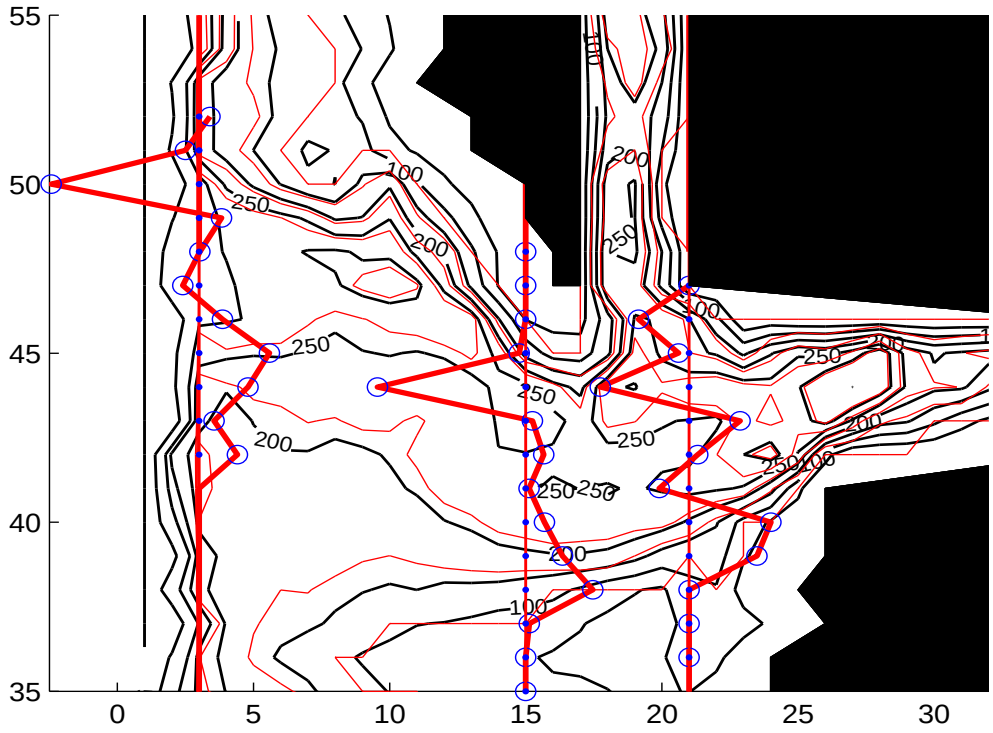

Figure 5.11: Volume transport over depth contours for a constant velocity of the WSC set to 0.25 ms^{-1}. Three cross sections of volume transport is plotted for x=3 (from y=42 to 52), x=15 (from y=35 to 48) and x=21 (y=36 to 47). Flow to the left of the zero line (at x = 3, 15 and 21) indicates outflow and the flow to the right of the line indicates inflow. The bold red line represents the volume transport. The blue dots on the zero lines (x = 3, 15 and 21) indicate the position where the volume transport, shown with blue circles, occurs. The streamlines (red contour lines) are drawn for the values of 0, -50, -100, -150 and -200.

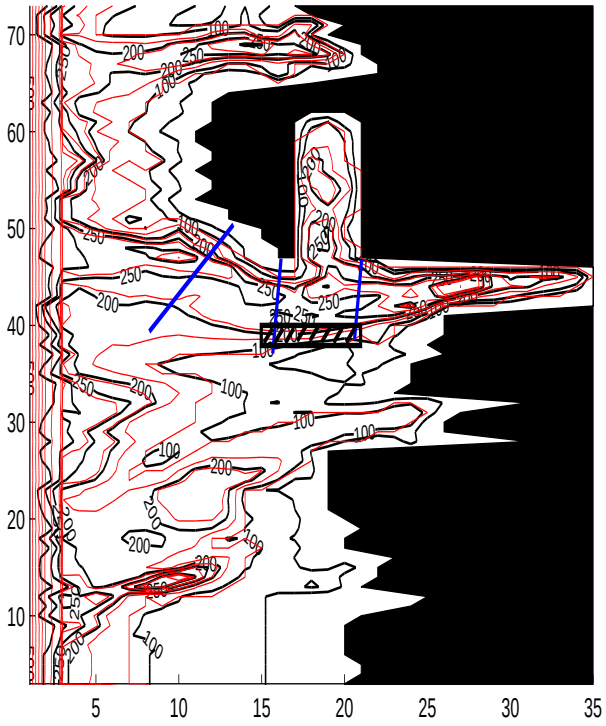

Figure 5.12: Streamlines for a WSC velocity of 0.25 ms^{-1}. The marked area is where the heat reduction is calculated, equal to an area of 192 km^2 and is calculated from $2 \triangle x \cdot 6 \triangle x$. Black lines represent the depth contours and the blue lines indicate the ADCP sections discussed in Section 2.3.2.

ocean i.e. upward heat flux. By knowing the volume transport, the temperature reduction due to the heat flux to the atmosphere can be calculated over a certain area, here A_0. The density is set to 1028 kgm^{-3} and the heat capacity equals 4000 J $kg^{-1}K^{-1}$. The calculated temperature reduction during 2007/2008 when the heat flux equalled -260 Wm^{-2}, equals 0.54°C. By choosing the heat flux to the atmosphere to be -220 W m^{-2}, as in 2008/2009, gives a temperature reduction of 0.46°C within A_0. Increasing the heat flux to the atmosphere to the maximum -500 Wm^{-2}, increases the temperature reduction for the marked area to 1.04°C.

Chapter 6

Discussion

6.1 Modelled circulation on the WSS

By solving the numerical equations in Chapter 4, the one layer model demonstrates how the inflow of warm and salty AW is topographically steered into the troughs, shelves and towards the fjords of western Spitsbergen. The WSC used in this model is derived from a linear current profile located with its maximum velocity over the 500 m isobath and a declining velocity towards shallower water. The boundary current in the model, representing the WSC, is in good agreement with observations from Teigen et al. [2010] and the chosen linear velocity profile demonstrates the influence of the WSC on the circulation over the shelf. By knowing that the mean half width of the WSC (Figure 4.2) is in the same range as the distance from the 500 m isobath and beyond the Isfjorden Trough entrance, inflow into the trough is expected. From the model results it is found that the inflow of AW into the troughs and on the shelf areas increases when the velocity of the WSC is increased from 0.20 ms^{-1} to 0.35 ms^{-1}. A 5% increase in the maximum WSC velocity from 0.21 ms^{-1} to 0.22 ms^{-1} yields a totally different picture of the topographically steered inflow. This is due to a surface elevation of ψ_0 setting up a flow over the shallower bathymetry contours which excites flow over a larger area on the shelf (Figure 5.5 and 5.6a).

Different flow branches are entering the Isfjorden and Kongsfjorden Troughs. It is demonstrated that a direct connection between the WSC and the troughs can be found. Especially the Isfjorden Trough has a direct communication with the WSC for most of the model data (Figures 5.5 to 5.8), indicating that the Isfjorden Trough has the largest possibility to connect to the WSC. This direct connection between the WSC and the trough is more moderate in the Kongsfjorden Trough, but it is still found for given WSC velocities between 0.27 ms^{-1} to 0.32 ms^{-1} (V_{wsc} = 0.28 ms^{-1} and 0.30 ms^{-1} are shown in Figures 5.7b and 5.7c, respectively). Another flow branch enters shallower areas at the upstream boundary and follows the isobaths north on the shelf, circulating within the troughs and continuing northwards. This branch is found to circulate Bredjupet or Bellsund before entering the Isfjorden Trough at shallower areas than the

direct inflow from the WSC. The more the velocity of the WSC increases the steeper topography the flow follows. From the Isfjorden Trough, water continues north on Forlandsbanken before entering the Kongsfjorden Trough, which is the most commonly observed inflow pathway into the Kongsfjorden Trough in the model data. AW from the WSC also enters the small trough west of Forlandsbanken, where the water flows northward and into the southern and middle part of the Kongsfjorden Trough entrance. Into the Isfjorden Trough a third branch of inflowing water is found close to the coast. When the velocity of the WSC gets large enough, water flows parallel to the coast entering the inner part of the trough where the mouth of Isfjorden is located (Figures 5.7d and 5.8a).

The model results give an overview of the troughs' communication with the WSC, and it is found that the WSC connects easier to the Isfjorden Trough than anywhere else on the shelf. The connection between the WSC and the Kongsfjorden Trough is only found with an increase in the WSC velocity from 0.27 ms^{-1} to 0.32 ms^{-1}. It is also seen that the inflow directly from the WSC into the Kongsfjorden Trough loses its connection earlier than what is observed for the Isfjorden Trough when the velocity of the WSC is increased. The topography in the outer part of the Kongsfjorden Trough has a small shallow bank between the outer part and the inner part of the trough. The small bank may provide some explanation as to why it is harder for the AW from the WSC to penetrate the Kongsfjorden Trough than the Isfjorden Trough.

By considering the streamlines (Figures 5.5 to 5.7) and the volume transport over the isobaths (Figure 5.10), it is found that the flow on the shelf follows steeper topography in the southern part of the Isfjorden Trough when the velocity of the WSC is increased. Increasing the velocity of the WSC is similar to an increase in the velocity scale, resulting in a relative increase in the relative vorticity part of

$$\bigtriangledown^2 \psi + \eta_B = \bigtriangledown^2 \psi + \frac{h_B}{\varepsilon D} = K(\psi), \tag{6.1}$$

letting the vorticity part be the dominant term of the equation. The topographical steering term, $\frac{h_B}{\varepsilon D}$, will decrease due to the increasing Rossby number, $\varepsilon = \frac{V_{wsc}}{fL}$. Gently sloping topography will therefore not be able to steer the flow since the vorticity dominates, while over steeper topography, where the topographical guiding is larger, the flow will be steered by topography. This is seen in Figure 5.10, where the maximum volume flow is drawn towards steeper topography when the velocity scale increases. The bottom topography is steeper at shallower depth in the southern part of the Isfjorden Trough.

Following the flow on the shelf with a constant maximum velocity of the WSC, in this case 0.25 ms^{-1} (Figure 5.11), the flow tends to be advected towards deeper topography when flowing eastward, on the southern side of the Isfjorden Trough. A faster flow increases the velocity shear and with only eastward flow the vorticity can be written as $\zeta = -\frac{\partial u}{\partial y}$. Thus, a larger velocity shear will increase the vorticity term in (6.1). To compensate the increasing vorticity along a streamline, the topographical steering term $\frac{h_B}{\varepsilon D}$, has to decrease by reducing h_B, to satisfy the

conservation of potential vorticity. A decrease in the topographical steering term will make the flow follow deeper isobaths. It is shown that when passing the steeper topography, south in the Isfjorden Trough, the maximum volume transport is found over the 100 to 150 m isobath (Figure 5.11), while further east the flows' maximum volume transport follows the 200 m isobath.

Southward transport is found in the entrance of the troughs in the current vector plots (Figures 5.8b and 5.8d), where the WSC velocity is set to 0.35 ms^{-1} and 0.36 ms^{-1}. As discussed above, when following a streamline, the vorticity changes depending on the bottom slope and the flow seeks deeper isobaths to compensate for the increase in vorticity. In the northern part of the Isfjorden Trough the isobaths are densely spaced leading to a faster flow. The flow is forced towards the flat seafloor where finally the only option for the flow is to move south. This southward flow is also found in moderate amount at the entrance of the troughs when we choose a WSC velocity of less than 0.35 ms^{-1}, representing a more or less closed circulation inside the troughs.

The model results can be used to explain the inflowing event into the Isfjorden Trough discussed by Cottier et al. [2007]. From 18 December 2005 to 24 January 2006 southerly winds and warming dominated the WSS, at the same time an inflow and accumulation of water could be detected in Isfjorden (see Cottier et al. [2007], Figure 3b). The southerly wind forces the surface water to stack up against the coast, setting up a pressure gradient force away from the coast in an offshore direction. The surface elevation discussed by Cottier et al. [2007], can be found in the model results where an increase in the velocity of the WSC gives an increase in the surface elevation. The southerly wind can also push the WSC eastward towards shallower areas (as observed in Figure 2.2a in December 2005), allowing the AW from the WSC to easier come in contact with the WSS and flow into the troughs or on the shelf west of Spitsbergen. The measured water temperature is consequently increasing during this period and interrupting the normal ice formation found at this time of the year. A strong southerly wind period is therefore able to increase and shift the WSC towards the shelf and our model shows that this will lead to an increased inflow of AW to the WSS. The modelled circulation pattern shows that AW is guided towards the fjords most efficiently in the troughs, which preconditioned the following inflow of AW to the fjords when the wind reversed and the WSS experienced strong northerly winds [Cottier et al., 2007].

Another example confirming the model results is shown in Figure 6.1. Here, AW is steered along the WSS and into the Isfjorden Trough given by the mean Sea Surface Temperature (SST) from satellite data (MODIS) for the two first weeks of January 2008. During January 2008, the WSC had a higher velocity maximum and a wider velocity profile (Figure 2.2b), and the respond on the shelf is easy to trace from the satellite data (Figure 6.1).

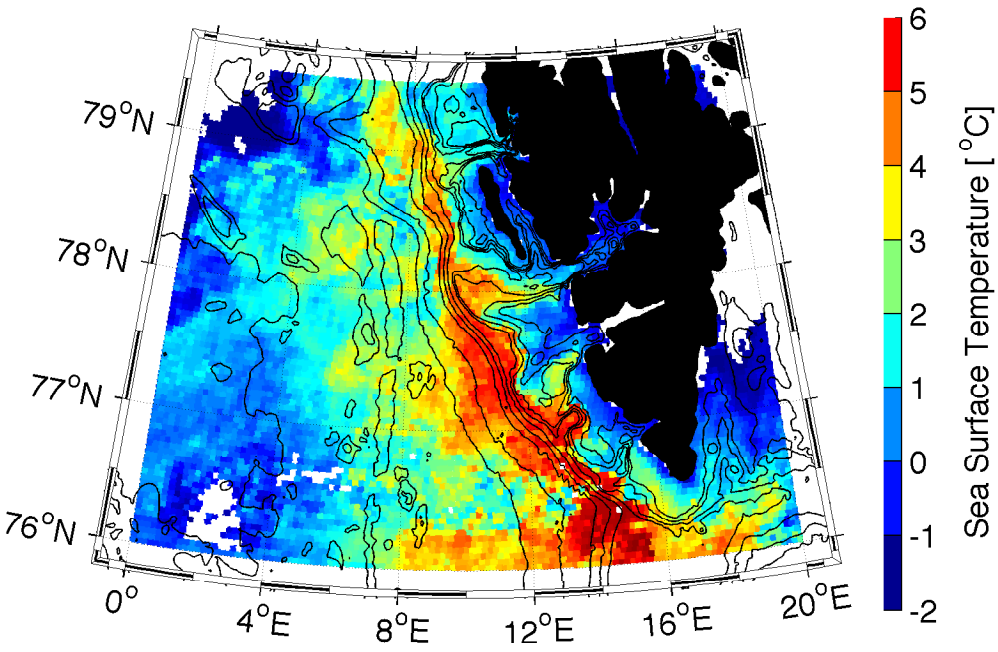

Figure 6.1: MODIS Sea Surface Temperature (SST) from the two first weeks of January 2008 taken over the Fram Strait and the WSS. Spitsbergen is located to the right. Reprojected MODIS SST data were kindly made available to us by A. Korosov and S.Sandven at the Nansen Environmental and Remote Sensing Center (NERSC).

6.2 The volume transport in and out of the Isfjorden Trough

The volume transport in the Isfjorden Trough is given in Table 5.2 and is calculated over the cross section marked with a red line in Figure 5.9. The net volume transport tends to vary between a net inflow and a net outflow, but the variations are small compared to the in- and outflow values. Since the volume transport should be conserved, we would expect the net flow to be zero. The volume transport is calculated over a mean depth between each grid point $\triangle y$, giving a certain error in the volume transport estimates. By choosing a better model resolution, the error could be reduced. Calculating the volume transport over a slope with a $\triangle H$ of 10 m could give an error estimate in order of 10 m^3s^{-1}. Choosing a $\triangle H$ of 20 m could give an error estimate in order of 100 m^3s^{-1}, while having a $\triangle H$ of 100 m could give error estimates on several 1000 m^3s^{-1}. This can be an explanation for the errors in the calculated net volume transport, where a larger error can be expected for calculations done over a steeper slope. However, looking at a WSC velocity from 0.34 ms^{-1} to 0.36 ms^{-1} the error in net volume transport increases to over 1000 m^3s^{-1}. We know from the discussion above that a third branch of inflow into the Isfjorden Trough is found along the coast, when the velocity of the WSC reaches 0.34 ms^{-1} or more. This flow is not captured by the cross section measuring the inflow, and an increase in outflow is therefore expected. The WSC velocity of 0.36 ms^{-1} gives a very large increase in net

inflow compared with a velocity of 0.35 ms^{-1}. If the velocity of 0.36 ms^{-1} gives representative results or not will be discussed in Section 6.3.

6.3 Limitations due to the simplified WSC used in the model

The WSC in the model needs to have a velocity between 0.21 ms^{-1} and 0.35 ms^{-1} to produce inflow of water into the troughs and onto the shelf area west of Spitsbergen. Velocities less than 0.20 ms^{-1} will lock the WSC to the continental slope. By knowing how far towards the coast a sea surface elevation is found, being the distance from origo to where the streamline profile crosses zero in Figure 5.3, it is possible to calculate the WSC velocity by (4.7). From Figure 2.2b the eastern half of the skewed WSC profile from January 2008 is estimated to be approximately 20 km. From January 2006 the WSC is found closer to the coast by at least 10 km, seen from Figure 2.2a. The 20 km width of the WSC during January 2008 corresponds to a streamline that would cross the zero line in $x = 0.25$ (multiplied by $L = 80$ km) in Figure 5.3, corresponding to a WSC velocity of 0.23 ms^{-1}. During January 2006, when the current is relocated further towards the coast, the streamline from Figure 5.3 will cross the zero line further towards the coast indicating a larger WSC velocity. Letting the current be relocated by 10 km towards the coast will give a streamline that crosses zero at $x \approx 0.38$, corresponding to a velocity of 0.25 ms^{-1}. The relocation of the WSC is the same as the displacement variable from the equations in Chapter 4, referred to as a. The WSC in the model is fixed over the seaward boundary on the 500 m isobath, and the displacement distance, a, is set to zero. By increasing a from zero the WSC will move closer to the coast and the observed situation from January 2006 can be interpreted by the model. But to change the location of the WSC closer to the coast, will give the same model results as an increase of the velocity of the WSC. We therefore concentrate on the velocity of the WSC and leave a unchanged. A velocity of the WSC of 0.23 ms^{-1} and 0.25 ms^{-1}, calculated from Figure 2.2, is in the range of the velocities used when running the model. Hence, the surface elevation set up by a 0.20 ms^{-1} to 0.25 ms^{-1} velocity range in the maximum velocity of the WSC give the most realistic flow response on the WSS.

By increasing the boundary current from 0.35 ms^{-1} to 0.36 ms^{-1}, a large change in the observed inflow is found from the model results (Figures 5.8c and 5.8d). The connection between the WSC found over the steeper slope and the eastward flow penetrating the troughs, is reduced. From streamlines and current vectors, a strong southward flow is observed in the trough entrances when the velocity of the WSC is set to 0.36 ms^{-1}, with flow crossing isobaths in several places. If the velocity of the WSC is further increased it will lose all its connection to the troughs and no inflow from the WSC will be observed. The model setup now represents more of a coastal current driven by a pressure gradient with water stacked up against the coast, than a direct inflow effect of the WSC; a similar case to what is discussed by Lagerloef [1983]. The model with a chosen boundary current equal to 0.36 ms^{-1} will not be discussed further as we set an upper limit where the model is valid at a WSC velocity of 0.35 ms^{-1}.

6.4 Heat loss estimates

The heat loss to the atmosphere due to different heat fluxes from the ocean to the atmosphere, is calculated in Section 5.3. Temperature reduction from the same area where the heat loss is calculated can be found from the winter CTD measurements, discussed in Section 2.3.1. The chosen area, A_0 (shaded area in Figure 5.12), corresponds approximately to the main inflow over the distance from the winter CTD section 2, station 194 to 195, to section 3, station 202 to 42, on the southern side of the Isfjorden Trough (Figures 2.7c and 2.7e). By averaging the temperature for the upper and lower depths, it is found that the temperature at the surface down to approximately 100 m, drops with 1°C to 2.3°C, while in the deeper part of the section the temperature drops approximately between 0.5°C and 0.8°C. Note that the modified AW that is found in the entire water column in section 2, is found below 150 m in section 3. The modified AW originates from AW that has been cooled down by the atmosphere and mixed with cooler, fresher water masses on the shelf. The calculated temperature losses differ for different heat flux values. Choosing a heat flux of -220 Wm^{-2} the temperature will drop 0.46°C. If the heat flux is -260 Wm^{-2} the temperature will drop 0.54°C and if we choose the maximum heat flux to be -500 Wm^{-2} the temperature will drop 1.04°C. The calculated heat reductions are less than those found from the CTD data, except when the heat flux to the atmosphere is chosen to be -500 Wm^{-2} or when looking at the minimum heat reduction from the CTD data. By knowing that the subsurface layer between 100 m and 500 m, of the upper slope domain of west Spitsbergen has a heat loss 2.5-3 times larger than the heat loss estimated for the upper 100 m surface layer [Saloranta and Haugan, 2004; Nilsen et al., 2006], a lower heat loss estimate is expected in this case compared to the calculated values in this thesis. Since we only look at the heat loss to the atmosphere, the heat loss to colder surrounding water masses is neglected, and hence, the large heat loss estimates below 100 m is not accounted for.

6.5 Model limitations

The model is based on a one layer barotropic situation which is observed for the southern part of the Isfjorden Trough during winter. A two layer system is observed from CTD data in the northern part of the trough during winter and also during summer (Figures 2.6 and 2.7). Only the WSC is used to run the model and is in this case the main source for all circulation of the WSS. As seen from Figure 2.1, a coastal current with colder Arctic Water is also observed close to the coast of Spitsbergen, as it flows around the south tip of Spitsbergen and follows the shelf area west of Spitsbergen northwards. This coastal current may act as a geostrophic control [Nilsen et al., 2008] at the fjord mouth, and will give a stratification which is not taken into account in this model. By neglecting this stratification, flow in the model has easier access to the inner part of the troughs where a front of colder and fresher water would normally be expected. The front could prevent AW from penetrating the Isfjorden mouth and the coastal current would be able to steer the incoming flow northward.

The westward and eastward flows resulting from the model are small compared to measured values found in the Isfjorden Trough (Figure 2.10). This has to do with the chosen WSC profile. Figure 4.2 indicates the region where the WSC affects the circulation on the shelf and where the relative vorticity is calculated. The modelled velocities are found to be in the same order as the velocities found in Figure 4.2a in the marked region indicated by a red line. Moreover, the WSC is the only source for the sea surface elevation. We also lack the pressure gradient force by water being stacked up against the coast.

The model's limitations for explaining the heat reduction are obvious. Knowing that the water column not only loses heat to the atmosphere, but also to the colder surrounding water, we expect the calculated heat loss values to be smaller than the observed ones. A correct estimate of the volume transport is also important since it can have a great effect on the heat calculations. By calculating a volume transport that is smaller than that of the true flow, the water mass would be given more time to pass the area and to lose more heat. A transport that is faster than that of the true flow will make the water flow so fast that only a small amount of heat is lost. Vertical heat loss within the water column is neglected due to the assumption of a one layer system with uniform temperature in the entire column.

Chapter 7

Summary and concluding remarks

A one layer model made by Nilsen and Vaardal-Lunde [2012] was used to model the steady barotropic velocity field by numerically solving the quasigeostrophic potential vorticity equation on a f-plane. The model was used to calculate the streamlines on the West Spitsbergen Shelf (WSS), demonstrating how the inflow of warm and salty AW is topographically steered into the troughs and onto the WSS. The homogeneous water column during winter fulfils the requirement of a one layer model. Since the WSC is highly barotropic, the barotropic assumption of the model is satisfied during winter time. The simple one layer barotropic model gives a good approximation of the dynamical processes on the WSS.

The model shows that an increase in the flow speed of the WSC will have an effect on the flow in the troughs and the shelf area within the modelled bathymetry. The WSC is found to connect easier to the Isfjorden Trough than anywhere else on the shelf, letting this trough be exposed to warm and salty water also during winter. Inflow is also observed into the Kongsfjorden Trough, but the connection directly to the WSC is not as pronounced here as in the Isfjorden Trough. By increasing the flow speed of the WSC, the vorticity term of the solved equation (6.1) increases and the flow needs to follow steeper topography in order to be topographically steered. This can be seen in both the streamline model results and the calculation of the volume transport. It is also found that the streamlines seek deeper isobaths when the vorticity increases for a constant WSC velocity, advecting the flow towards deeper isobaths on its way around the trough.

The heat loss to the atmosphere can be derived from the conservation of heat (3.22). The calculated heat reduction is found to be smaller than the observed heat reduction from the CTD data, which we expect since we are only looking at heat loss to the atmosphere.

Further work needs to be done to improve the model. By extending the model formulation to a two layer system, the mentioned coastal current and stratification can be taken into account. By adding stratification in the model, the model will give a more correct result for the northern part of the trough during winter. Circulation patterns during summer can then also

be studied. To improve the heat loss estimates, heat loss can be calculated for the whole water column, also taking heat loss to surrounding water masses into account. The heat loss to the atmosphere calculated in this thesis gives an under estimated heat loss and is therefore not an accurate result.

The simple one layer model used in this thesis can give a better overview of how the circulation on the WSS is affected by the WSC. The results are compared with the inflow situation discussed by Cottier et al. [2007], where the model data can be used to explain the inflow observed into the Isfjorden Trough. By knowing more about the circulation in the troughs and on the shelf west of Spitsbergen, more can be said about the heat loss of the WSC on its way to the Arctic, which is an important factor for understanding the Arctic heat budget and the recent warming of the Arctic Ocean.

Bibliography

Blindheim, J. and Østerhus, S. [2005], 'The Nordic Seas, main oceanographic features', *The Nordic seas: an integrated perspective: oceanography, climatology, biogeochemistry, and modeling* p. 11.

Boyd, T. and D'Asaro, E. [1994], 'Cooling of the West Spitsbergen Current: Wintertime observations west of Svalbard (Paper 94JC01824)', *Journal of Geophysical Research-Part C-Oceans-Printed Edition* **99**(11), 22597–22618.

Cokelet, E., Tervalon, N. and Bellingham, J. [2008], 'Hydrography of the West Spitsbergen Current, Svalbard Branch: Autumn 2001', *Journal of Geophysical Research* **113**(C1), C01006.

Cottier, F., Nilsen, F., Inall, M., Gerland, S., Tverberg, V. and Svendsen, H. [2007], 'Wintertime warming of an Arctic shelf in response to large-scale atmospheric circulation', *Geophysical Research Letters* **34**(10), L10607.

Cottier, F., Tverberg, V., Inall, M., Svendsen, H., Nilsen, F. and Griffiths, C. [2005], 'Water mass modification in an Arctic fjord through cross-shelf exchange: The seasonal hydrography of Kongsfjorden, Svalbard', *Journal of Geophysical Research* **110**, C12005.

Fahrbach, E., Meincke, J., Østerhus, S., Rohardt, G., Schauer, U., Tverberg, V. and Verduin, J. [2001], 'Direct measurements of volume transports through Fram Strait', *Polar Research* **20**(2), 217–224.

Gascard, J., Richez, C. and Rouault, C. [1995], 'New insights on large-scale oceanography in Fram Strait: the West Spitsbergen Current', *Arctic oceanography, marginal ice zones and continental shelves* **49**, 131–182.

Jakobsson, M., Macnab, R., Mayer, L., Anderson, R., Edwards, M., Hatzky, J., Schenke, H. and Johnson, P. [2008], 'An improved bathymetric portrayal of the Arctic Ocean: Implications for ocean modeling and geological, geophysical and oceanographic analyses', *Geophys. Res. Lett* **35**(4), L07602.

Kundu, P. [1990], *Fluid mechanics*, Academic Press, San Diego.

Lagerloef, G. [1983], 'Topographically controlled flow around a deep trough transecting the shelf off Kodiak Island, Alaska', *Journal of Physical Oceanography* **13**, 139–146.

Manley, T. [1995], 'Branching of Atlantic Water within the Greenland-Spitsbergen Passage: an estimate of recirculation', *Journal of Geophysical Research* **100**(C10), 20627.

Nilsen, F., Cottier, F., Skogseth, R. and Mattsson, S. [2008], 'Fjord-shelf exchanges controlled by ice and brine production: The interannual variation of Atlantic Water in Isfjorden, Svalbard', *Continental Shelf Research* **28**(14), 1838–1853.

Nilsen, F., Gjevik, B. and Schauer, U. [2006], 'Cooling of the West Spitsbergen Current: Isopycnal diffusion by topographic vorticity waves', *Journal of Geophysical Research* **111**(C8), C08012.

Nilsen, F. and Vaardal-Lunde, J. [2012], 'A Simple Topographically Controlled Shelf Circulation Model - Intrusion of Atlantic Water on an Arctic Shelf', *In preparation.* .

Pedlosky, J. [1987], *Geophysical fluid dynamics*, 2d edn, Springer-Verlag, New York.

Polyakov, I., Timokhov, L., Alexeev, V., Bacon, S., Dmitrenko, I., Fortier, L., Frolov, I., Gascard, J., Hansen, E., Ivanov, V. et al. [2010], 'Arctic ocean warming contributes to reduced polar ice cap', *Journal of Physical Oceanography* .

Press, W., Flannery, B., Teukolsky, S., Vetterling, W. et al. [2007], *Numerical recipes*, Vol. 3, Cambridge university press Cambridge.

Saloranta, T. [2001], 'Hydrographic structure of the sea west of Svalbard along and across the continental slope. Reports in Meteorology and Oceanography 2', *Geophysical Institute, University of Bergen* .

Saloranta, T. and Haugan, P. [2001], 'Interannual variability in the hydrography of Atlantic water northwest of Svalbard', *Journal of Geophysical Research* **106**(C7), 13931.

Saloranta, T. and Haugan, P. [2004], 'Northward cooling and freshening of the warm core of the West Spitsbergen Current', *Polar Research* **23**(1), 79–88.

Saloranta, T. and Svendsen, H. [2001], 'Across the Arctic front west of Spitsbergen: high resolution CTD sections from 1998-2000', *Polar Research* **20**(2), 177–184.

Schauer, U., Beszczynska-Möller, A., Walczowski, W., Fahrbach, E., Piechura, J. and Hansen, E. [2008], 'Variation of measured heat flow through the Fram Strait between 1997 and 2006', *Arctic-Subarctic Ocean Fluxes: Defining the Role of the Northern Seas in Climate* pp. 65–85.

Schauer, U., Fahrbach, E., Osterhus, S. and Rohardt, G. [2004], 'Arctic warming through the Fram Strait: Oceanic heat transport from 3 years of measurements', *Journal of geophysical research* **109**(C6), C06026.

Svendsen, H., Beszczynska-Möller, A., Hagen, J., Lefauconnier, B., Tverberg, V., Gerland, S., Ørbæk, J., Bischof, K., Papucci, C., Zajaczkowski, M. et al. [2002], 'The physical environment

of Kongsfjorden–Krossfjorden, an Arctic fjord system in Svalbard', *Polar research* **21**(1), 133–166.

Swift, J. and Aagaard, K. [1981], 'Seasonal transitions and water mass formation in the Iceland and Greenland seas', *Deep Sea Research Part A. Oceanographic Research Papers* **28**(10), 1107–1129.

Teigen, S. [2011], Water mass exchange in the sea west of Svalbard, A process study of flow instability and vortex generated heat fluxes in the West Spitsbergen Current, PhD thesis, University of Bergen, Norway.

Teigen, S., Nilsen, F. and Gjevik, B. [2010], 'Barotropic instability in the West Spitsbergen Current', *Journal of Geophysical Research* **115**(C7), C07016.

Zhang, J., Rothrock, D. and Steele, M. [1998], 'Warming of the Arctic Ocean by a strengthened Atlantic inflow: Model results', *Geophysical Research Letters* **25**(10), 1745–1748.